Dorsoventral-mediated *Shh* induction is required for axolotl limb regeneration

Sakiya Yamamoto[1], Saya Furukawa[1], Ayaka Ohashi[1], Mayuko Hamada [1, 2], and Akira Satoh[1]

Affiliations:

[1] Okayama University, Graduate School of Environmental, Life, Natural Science and Technology, Okayama, Japan

[2] Ushimado Marine Institute (UMI), Okayama University, Okayama, Japan

*Corresponding author

Akira Satoh, Ph.D.,

Okayama University, Okayama University, Graduate School of Environmental, Life, Natural Science and Technology

Email: satoha@cc.okayama-u.ac.jp

Tel: +81-86-251-8421

Abstract

Axolotls (*Ambystoma mexicanum*) exhibit a remarkable ability to regenerate limbs after amputation. Classical experiments have suggested that contact between cells derived from distinct orientations—dorsal, ventral, anterior, and posterior—within the regenerating blastema is necessary for accurate limb pattern formation. However, the molecular basis for this requirement has remained largely unknown. Here, we demonstrate that both dorsal and ventral tissues are required for limb formation via induction of *Shh* expression, which plays a crucial role in limb patterning. Using the accessory limb model (ALM), we induced position-specific blastemas lacking cells derived from a single orientation (anterior, posterior, dorsal, or ventral). Patterned limb formation occurred only in blastemas containing both dorsal- and ventral-derived cells. We further observed that *Shh* expression requires dorsoventral contact within a blastema, highlighting the necessity of dorsoventral contact for inducing *Shh* expression. In addition, we identified WNT10B and FGF2 as dorsal- and ventral-mediated signals, respectively, that create the inductive environment for *Shh* expression. Our findings clarify the role of dorsal and ventral cells in inducing *Shh*, a mechanism that has rarely been studied in the context of limb regeneration and pattern formation. This model provides new insights into how cells with different positional identities drive the regeneration process.

Introduction

Axolotls (*Ambystoma mexicanum*) possess remarkable regenerative abilities, enabling the regeneration of entire limbs after amputation. Among tetrapods (four-limbed vertebrates), only urodele amphibians retain the lifelong ability to regenerate fully developed limbs. Investigating the molecular mechanisms underlying axolotl limb regeneration could provide valuable insights for advancing regenerative medicine in humans, potentially leading to new therapies for tissue repair and organ regeneration.

The limb regeneration process can be divided into two stages: the blastema (regenerating limb primordium) induction process and the limb patterning process. The induction of a blastema, which contains highly proliferative multipotent and unipotent cells, depends on the presence of nerves at the injured region; when a denervated limb is amputated, a blastema is not induced (Todd, 1823). This blastema induction process is followed by the limb patterning process. The limb patterning process has been considered to be mainly a recapitulation of limb development. Actually, activation of many developmental genes can be found during this phase. Such sequential events accomplish axolotl limb regeneration.

To accomplish limb patterning, cells need to know its address within a limb and exert its position specific role. Such address of cells has been referred as positional identities. In limb development/regeneration, positional identities are thought to be established along three-dimensional axes—anteroposterior, dorsoventral, and proximodistal. In amniote limb development, WNT7A, secreted from dorsal ectoderm, induces *Lmx1b* expression in the underlying mesenchyme, thereby specifying dorsal identity (Riddle et al., 1995; Vogel et al., 1995; Cygan et al., 1997; Chen et al., 1998; Chen, 2002). On the ventral side, the ventral identity is specified indirectly by *En1*, which is expressed in the ventral ectoderm, restricts *Wnt7a* expression to the dorsal ectoderm and thereby prevents induction of *Lmx1b* in the ventral mesenchyme (Loomis et al., 1996; Logan et al., 1997; Chen and Johnson, 2002). Similarly, SHH is known to regulate anteroposterior patterning (Riddle et al., 1993). In axolotl limb regeneration, the establishment of the dorsoventral positional identities is still largely unknown, except for dorsal-specific *Lmx1b* expression (Shimokawa et al., 2013). Regarding the anteroposterior axis, *Shh* expression is highly conserved and restricted to the posterior margin. Though the process of the establishment of the positional identities is still veiled in axolotl limb regeneration, it is apparent that the regeneration blastema possesses regional specificity.

For successful limb patterning in limb regeneration, interactions between anterior, posterior, dorsal, and ventral cells within a blastema have been considered essential. The importance of these interpositional interactions was investigated in creating double-half limbs. Amputating the double-half limbs can provide a blastema in a “one-positional-identity-missing” state. For example,

when a double-dorsal limb—a chimeric limb surgically generated by excising the ventral half and replacing it with a dorsal half from the contralateral limb while preserving anteroposterior orientation—is amputated, the resulting blastema lacks ventral positional identity. Such blastemas lacking one positional identity can form hypomorphic, spike-like structures or fail to regenerate; in other cases, they regenerate limbs with complete anteroposterior axes accompanied by symmetric dorsoventral duplications (Bryant, 1976; Bryant and Baca, 1978; Burton et al., 1986). It is noteworthy that, in the non-regenerating cases, structural patterns along the anteroposterior axis appear to be lost even though both anterior and posterior cells should, in principle, be present in a blastema induced from a double-half limb. These observations are consistent with the idea that, during axolotl limb regeneration, signals mediated by dorsal cells must act on ventral cells, and signals mediated by ventral cells must act on dorsal cells, during the limb patterning process. In contrast, in amniote limb development, *Wnt7a*/*Lmx1b* or *En1* mutants show that limbs can exhibit anteroposterior patterning even when tissues are dorsalized or ventralized—i.e., in the relative absence of ventral or dorsal cells, respectively (Riddle et al., 1995; Chen et al., 1998; Loomis et al., 1996). Taken together, these findings indicate that the mechanism underlying limb patterning during axolotl regeneration differs from that operating during amniote limb development. Additional experiments involving ectopic contact between opposite regions (e.g., anterior-posterior or dorsal-ventral) of a blastema further support the critical role of interpositional interactions in the limb patterning process, as such interactions can lead to ectopic limb formation (Iten and Bryant, 1975; Bryant and Iten, 1976; Maden, 1980; Stocum, 1982). These findings suggest that signals mediated by each positional identity are required for successful limb patterning, such that the absence of any one of them leads to failure. To further understand limb regeneration, the molecular basis of these positional identity-mediated signals in limb patterning process should be elucidated.

The accessory limb model (ALM), a non-amputation experimental system, provides a valuable approach for studying axolotl limb regeneration, particularly the role of interpositional interactions (Endo et al., 2015). In this model, a blastema is induced through skin wounding combined with nerve deviation (Endo et al., 2004, Satoh et al., 2007). When ALM surgery is performed on the anterior side, the induced blastema (ALM blastema) lacks posterior-derived cells and is unable to form a properly patterned limb. This limitation can be overcome by supplying posterior-derived cells via a skin graft from the posterior side, enabling the successful regeneration of a patterned limb. Similarly, an ALM surgery can be performed on the posterior, dorsal, or ventral side of a limb; in each case, the induced ALM blastema is expected to lack cells from the corresponding opposite orientation (anterior, ventral, or dorsal, respectively). This condition allows the investigation of blastema induction and limb patterning by selectively removing cells from

specific orientations of the limb. Analyzing the characteristics and developmental limitations of these ALM blastemas provides valuable insights into the positional identity-mediated signals that regulate axolotl limb regeneration.

The molecular basis of the interpositional interactions within a blastema in the limb patterning process has been partially elucidated (Nacu et al., 2016). In a normal blastema, *Fgf8* and *Shh* are expressed at the anterior and the posterior regions, respectively. A previous study demonstrated that FGF8 and SHH proteins can substitute for anterior and posterior tissues, respectively, to form a patterned limb. Moreover, these proteins function as mutually inductive signals, maintaining each other's expression. These findings suggest that FGF8 and SHH serve as the anterior- and posterior-mediated signals, respectively. In contrast, the molecular basis of dorsal- and ventral-mediated signals remains poorly understood. Previous studies have shown that retinoic acid supplementation can convert the dorsal identity to the ventral, enabling patterned limb formation even in the absence of ventral tissues (McCusker et al., 2014; Ludolph et al 1990; Vieira et al., 2019). However, the ventral-mediated signal remains uncertain, as retinoic acid induces ventral positional identities rather than acting as the ventral-mediated signal itself, suggesting the existence of another, downstream ventral-mediated signal. Consequently, the mechanisms underlying dorsal- and ventral-mediated signals, as well as how they relate to the anterior- and posterior-mediated signals (FGF8 and SHH, respectively), remain unclear.

In the present study, we investigate the roles of dorsal- and ventral-mediated signals in limb patterning. We confirmed the necessity of dorsoventral tissue contact for limb patterning using the ALM. We found that the induction of *Shh* expression was dependent on the co-existence of dorsal and ventral cells in axolotl limb regeneration. Furthermore, we identified WNT10B and FGF2 as dorsal- and ventral-mediated signals, respectively, by RNA-seq analysis, and confirmed that these factors mediate *Shh* expression in axolotl blastemas. Our results suggest that the crucial role of the dorsal- and ventral-mediated signals in the limb patterning process is to induce *Shh* expression, thereby enabling anteroposterior interaction. These results contribute to understanding how the integration of four positional identities—dorsal, ventral, anterior, and posterior—drives proper limb patterning during axolotl limb regeneration.

Results

Dorsoventral tissue contact is required for limb regeneration in the ALM

We performed the ALM experiment on *Ambystoma mexicanum* to directly test whether dorsoventral tissue contact, as well as anteroposterior tissue contact, is required for limb patterning (Fig. 1). The skin was removed from one side (anterior, posterior, dorsal, or ventral) of a limb, and the large nerve fibers running along the center of a limb (*Nervus medianus* and *Nervus ulnaris*, Fig. 1A) were dissected and rerouted to the wounded region. We supplied the cells from the contralateral side of a limb as a skin graft in experimental conditions to ensure the presence of sufficient cells for patterned limb formation. We conducted eight types of ALM blastema inductions, which can be categorized into two groups: basic ALM blastemas and skin-grafted ALM blastemas. The basic ALM blastemas included the anteriorly induced ALM blastema (AntBL), the posteriorly induced ALM blastema (PostBL), the dorsally induced ALM blastema (DorBL), and the ventrally induced ALM blastema (VentBL), all of which should lack cells from the contralateral side. The skin-grafted ALM blastemas included AntBL with posterior skin grafting (AntBL+P), PostBL with anterior skin grafting (PostBL+A), DorBL with ventral skin grafting (DorBL+V), and VentBL with dorsal skin grafting (VentBL+D); these ALM blastemas should contain cells with all anteroposterior and dorsoventral orientations. For the ALM experiment, we defined the two large blood vessels running on the anterior and posterior sides at the stylopod level (*Vena cephalica* and *Vena. basilica*, Fig. 1A) as the anterior and posterior dorsoventral borders, respectively. At 10 days post-surgery (dps), an ALM blastema was observed in all experimental groups (Fig. 1B–I). Consistent with previous studies (Endo et al., 2004; Nacu et al., 2016), limbs with multiple digits were formed from AntBL+P and PostBL+A (Table 1, Fig. 1F, G), whereas AntBL and PostBL either regressed or formed bump structures (Table 1, Fig. 1B, C). Similarly, DorBL+V and VentBL+D formed limbs (Table 1, Fig. 1H, I), whereas most DorBL and VentBL either regressed or formed bump structures (Table 1, Fig. 1D, E). Notably, only 1 out of 12 DorBL formed a limb, which may have resulted from ventral tissue contamination, as the rerouted nerves originally ran along the ventral side of the humerus. In contrast, none of the 22 VentBL formed multi-digit limbs. These results suggest that both dorsal and ventral tissues, as well as anterior and posterior tissues, are required for successful limb formation.

Gene expression patterns in ALM blastemas

To elucidate the characteristics of the ALM blastemas that typically fail to form limbs (AntBL, PostBL, DorBL, and VentBL), we analyzed gene expression patterns at 10 dps (Fig. 2, Fig. S1). *Lmx1b*, a gene necessary and sufficient for establishing the dorsal identity in mesenchymal cells in developing limb buds (Vogel et al., 1995; Chen et al., 1998; Chen, 2002), was used as a dorsal marker because we previously reported that *Lmx1b* is exclusively expressed in dorsal-derived cells and can be activated in the ALM experiment (Iwata et al., 2020; Yamamoto et al., 2022). The

173 expression patterns of *Fgf8*, *Shh*, and *Lmx1b* were investigated using *in situ* hybridization (ISH). In
174 AntBL and PostBL, *Lmx1b* expression was restricted to the dorsal half of the blastemas (Fig. 2B, G,
175 Fig. S1A, D, n=5/5 for both), suggesting the presence of both dorsal and ventral tissues. These
176 expression patterns correspond to the anatomically defined dorsoventral borders (Fig. 1A). In
177 contrast, *Lmx1b* was expressed throughout the entire region of DorBL (Fig. 2L, Fig. S1G, n=6/6),
178 whereas no *Lmx1b* expression was detected in VentBL (Fig. 2Q, Fig. S1J, n=6/6), suggesting the
179 absence of ventral tissue in DorBL and dorsal tissue in VentBL. Consistent with previous studies,
180 *Fgf8* expression was observed in AntBL (Fig. 2C, Fig. S1B, n=4/5), but not in PostBL (Fig. 2H, Fig.
181 S1E, n=5/5, Nacu et al., 2016). Conversely, *Shh* expression was detected in PostBL (Fig. 2I, Fig.
182 S1F, n=5/5), but not in AntBL (Fig. 2D, Fig. S1C, n=5/5). In DorBL and VentBL, *Shh* expression
183 was largely absent (Fig. 2N, Fig. S1I, n = 5/6; Fig. 2S, Fig. S1L, n = 6/6), whereas *Fgf8* expression
184 was present in both (Fig. 2M, Fig. S1H, n=4/6; Fig. 2R, Fig. S1K, n=4/6). In DorBL, *Shh* expression
185 was observed in only 1 out of 6 samples, possibly due to ventral tissue contamination, as described
186 above. These results suggest that *Fgf8* expression is independent of the co-existence of dorsal and
187 ventral tissues, whereas *Shh* expression appears to require their presence.
188
189 ***Induction of Shh expression requires both dorsal and ventral cells***
190 The absence of *Shh* expression in most DorBL and VentBL, combined with its consistent expression
191 in all PostBL—which contain both *Lmx1b*-positive and *Lmx1b*-negative regions—suggests that the
192 induction of *Shh* expression depends on the presence of both dorsal and ventral cells (Fig. 2). To test
193 this hypothesis, we performed cell-tracing experiments using GFP-expressing skin from transgenic
194 animals (Fig. 3). We induced VentBL in leucistic animals and then grafted the posterior half of the
195 dorsal skin (VentBL+PD_{gfp}) or the posterior half of the ventral skin (VentBL+PV_{gfp}) from GFP
196 transgenic animals (Fig. 3A). Similarly, DorBL was induced in wild-type animals, and the posterior
197 half of the dorsal skin (DorBL+PD_{gfp}) or the posterior half of the ventral skin (DorBL+PV_{gfp}) from
198 GFP transgenic animals was grafted (Fig. 3A). GFP-positive mesenchymal cells derived from the
199 posterior skin were expected to express *Shh* if provided with a suitable environment, because
200 posteriorly derived cells, not anteriorly derived cells are known to have the competency to express
201 *Shh* in a blastema—i.e., whether a cell is capable of expressing *Shh* depends on its original positional
202 identity (Iwata et al., 2020), but whether it actually expresses *Shh* should depend on the environment
203 in which the cell is placed. If the induction of *Shh* expression depends on the co-existence of dorsal
204 and ventral cells, *Shh* expression in the GFP-positive cells should be observed in VentBL+PD_{gfp} and
205 DorBL+PV_{gfp} but not in DorBL+PD_{gfp} or VentBL+PV_{gfp}. Samples were collected at 10 dps, and the
206 expression of *Shh* and *Lmx1b* was analyzed using ISH. In all four experimental groups, *Lmx1b*

207 expression patterns in the GFP-negative regions were consistent with those in DorBL and VentBL
208 (Fig. 3D, F, H, J). In DorBL+PD$_{gfp}$ and VentBL+PD$_{gfp}$, *Lmx1b* expression was observed in GFP-
209 positive mesenchymal cells, whereas GFP-positive cells in DorBL+PV$_{gfp}$ and VentBL+PV$_{gfp}$ were
210 *Lmx1b*-negative (Fig. 3C–F). These *Lmx1b* expression patterns suggest that dorsoventral tissue
211 contact was present in VentBL+PD$_{gfp}$ and DorBL+PV$_{gfp}$ but absent in DorBL+PD$_{gfp}$ and
212 VentBL+PV$_{gfp}$. In the GFP-positive cells derived from PD$_{gfp}$ skin, *Shh* expression was observed in
213 VentBL+PD$_{gfp}$ (Fig. 3C, n=4/6) but not in DorBL+PD$_{gfp}$ (Fig. 3E, n=6/6). Similarly, in the GFP-
214 positive cells derived from PV$_{gfp}$ skin, *Shh* expression was observed in DorBL+PV$_{gfp}$ (Fig. 3I, n=3/6)
215 but not in VentBL+PV$_{gfp}$ (Fig. 3G, n=7/7). In addition, *Shh* expression was observed in some GFP-
216 negative mesenchymal cells in samples where *Shh* expression was observed in GFP-positive cells.
217 These results suggest that the induction of *Shh* expression in posteriorly derived cells requires the
218 co-existence of dorsal and ventral cells.
219
220 ***Limb formation in the absence of dorsoventral tissue contact***
221 DorBL and VentBL failed to form limbs (Fig. 1D, E). *Shh* expression was absent in these blastemas,
222 whereas *Fgf8* was expressed (Fig. 2). Results from the cell-tracing experiments suggest that *Shh*
223 expression requires the co-existence of dorsal and ventral cells (Fig. 3). Based on these findings, we
224 hypothesized that while the co-existence of dorsal and ventral cells is necessary to induce *Shh*
225 expression, it is not directly required for limb patterning if SHH protein is externally provided. To
226 test this hypothesis, we overexpressed *Shh* in DorBL and VentBL (Fig. 4A, B). As a positive control,
227 *Shh* was overexpressed in AntBL, where *Fgf8* was expressed but *Shh* expression was absent (Fig.
228 2C, D), because a previous study has shown that *Shh* overexpression to AntBL can induce limb
229 patterning (Nacu et al., 2016). As a result, *Shh*-electroporated AntBL, DorBL, and VentBL formed
230 limbs (n=10/19, 6/18, and 8/14, respectively, Fig. 4C–G). In contrast, GFP-electroporated DorBL
231 and VentBL (negative controls) failed to form limbs (n=7/7 and 6/6, respectively). We further
232 analyzed the anatomy of the induced limbs (Fig. 4H–K, Fig. S2). Because ALM-induced limbs
233 frequently exhibit abnormal and highly variable morphologies, which makes it difficult to use
234 consistent anatomical landmarks such as particular digits or muscle groups, we focused our analysis
235 on morphological symmetry. We found that limbs formed from DorBL and VentBL exhibited
236 symmetric structures along the dorsoventral axis, suggesting double-dorsal and double-ventral
237 structures, respectively (Fig. 4J, K, Fig. S2C, D). In contrast, limbs formed from AntBL, which
238 contained both *Lmx1b*-positive and *Lmx1b*-negative regions (Fig. 2B), exhibited asymmetric
239 structures similar to those of normal limbs (Fig. 4H, I, Fig. S2A, B). To evaluate the symmetry of the
240 limbs, we applied a machine learning-based method using ilastik because staining intensity varied

among samples, such that a region identified as “muscle” in one sample could be assigned differently in another if classification were based solely on color. The machine-learning classifier trained separately for each sample allowed us to group the same tissues consistently within that sample irrespective of intensity differences. To minimize the effects of curvature or fixation-induced distortion, the boxes with a width of 400 μm were selected, and the angle was adjusted so that the outer contour (epidermal surface) was aligned symmetrically; this procedure was applied uniformly across all conditions to avoid bias. Each pixel in the images was classified into five classes (Classes 1 to 5, Fig. 4L). In this process, we annotated regions of background (Class 1), cartilage (Class 2), muscle (Class 3), other connective tissue (Class 4), and epidermis (Class 5) as training data for classification. Using these annotated regions as references, pixels were automatically classified into the five classes. Each class was assumed to primarily represent these tissues and regions with similar characteristics. Symmetry scores were then calculated for each class individually and for the combined set of all classes (Fig. 4M–R, see Materials and Methods). The analysis revealed that symmetry scores for Classes 2 and 3, which encompass cartilage and muscle, and scores for the combined set of all classes were significantly higher in limbs formed from DorBL and VentBL compared to intact limbs (Fig. 4N, O, R). In contrast, the differences in symmetry scores for Classes 1, 4, and 5 in these limbs were relatively small (Fig. 4M, P, Q), likely because the axis of symmetry was manually set to maximize the external shape as symmetrically as possible. No significant differences in symmetry scores across all classes were observed between intact limbs and limbs formed from AntBL. These results suggest that limbs formed from DorBL and VentBL exhibit symmetric internal structures compared to normal limbs. Therefore, *Shh* overexpression appears to compensate for the lack of co-existence of dorsal and ventral cells in limb patterning, without inducing new dorsal or ventral identities. Thus, we conclude that the co-existence of both dorsal and ventral cells is critical for inducing *Shh* expression, which in turn is essential for limb patterning.

The molecular basis of the dorsal-mediated and ventral-mediated signals

To investigate the molecular basis of dorsal- and ventral-mediated signals, we performed RNA-seq analysis on DorBL and VentBL and identified differentially expressed genes (DEGs) between the two groups ($p < 0.05$, Fig. 5A). Among the DEGs, we specifically focused on genes annotated as “intercellular signaling molecules” in PANTHER and identified 21 genes (Fig. 5B). In this analysis, we found that 5 genes were expressed at higher levels in DorBL and 16 genes were expressed at higher levels in VentBL (Fig. 5B). Notably, *Wnt4*, *Wnt10b*, *Fgf2*, *Fgf7*, and *Tgfb2*, which encode secreted proteins, belong to the WNT, FGF, and TGFB families, which play key roles in major signaling pathways regulating limb developmental processes and we focused on these 5 genes. To

275 examine whether these genes regulate the induction of *Shh* expression in ALM blastemas, we
276 overexpressed each gene in either DorBL or VentBL. As a result, *Shh* expression was observed in
277 *Wnt10b*-electroporated VentBL (n=4/5) and *Fgf2*-electroporated DorBL (n=5/7, Fig. 5C). In contrast,
278 *Shh* expression was not detected in *Wnt10b*-electroporated DorBL (n=6/6) or *Fgf2*-electroporated
279 VentBL (n=5/5). Similarly, *Shh* expression was not detected in *Fgf7*- or *Tgfb2*-electroporated DorBL
280 (n=5/5 for both) or in *Wnt4*-electroporated VentBL (n=6/6). To confirm the ISH data, we performed
281 RT-qPCR on *Fgf2*- or GFP (control)-electroporated DorBL and *Wnt10b*- or GFP (control)-
282 electroporated VentBL and observed significant upregulation in *Shh* expression (Fig. 5D, E). In
283 *Wnt10b*-electroporated VentBL, *Axin2*, a downstream transcriptional target of canonical WNT
284 signaling, and *Lef1*, a canonical WNT pathway effector expressed in axolotl limb mesenchyme
285 (Glotzer et al., 2022), were also upregulated (Fig. 5F, G). Next, to confirm *Shh* induction by WNT
286 signaling in VentBL, we treated VentBL with 1 μM 6-bromoindirubin-3-oxime (GSK-3 Inhibitor,
287 BIO). As a result, *Shh* expression was relatively higher in BIO-treated VentBL compared to DMSO-
288 treated control VentBL (Fig. S3B, D, E). Additionally, symmetric limbs were formed in *Wnt10b*-
289 electroporated VentBL (n=3/12), BIO-treated VentBL (n=3/8), and in *Fgf2*-electroporated DorBL
290 (n=5/10), consistent with the results of *Shh* overexpression (Fig. 5H–J, Fig. S3A, C, F–H, Fig. S4A,
291 B). These findings suggest that WNT10B, expressed highly in dorsal blastema cells, and FGF2,
292 expressed highly in ventral blastema cells, function as the dorsal- and ventral-mediated signals,
293 respectively, to induce *Shh* expression, which subsequently supports limb patterning.
294 To test whether our model applies to normal regeneration, we analyzed *Wnt10b* and *Fgf2*
295 expression in amputation-induced blastemas (Fig. S5). We first performed *in situ* hybridization on
296 blastemas at several stages (early bud [EB], middle bud [MB], and late bud [LB]), but the signals
297 were weak and inconsistent, and we could not reliably detect clear expression domains (Fig. S5A).
298 We then performed RT-qPCR on manually microdissected dorsal and ventral halves of MB
299 blastemas (Fig. S5B). We found that *Wnt10b* and *Fgf2* were expressed at significantly higher levels
300 in the dorsal and ventral halves, respectively, compared to the opposite half. This dorsoventral-
301 biased expression of *Wnt10b* and *Fgf2* is consistent with our RNA-seq data from ALM blastemas.
302 We next quantified *Wnt10b*, *Fgf2*, and *Shh* expression across stages (intact, EB, MB, LB, and early
303 digit [ED]) and found that *Wnt10b* and *Fgf2* expression peaked at the MB stage, whereas *Shh*
304 expression peaked later, at the LB stage (Fig. S5C). This temporal offset in *Shh* upregulation relative
305 to *Wnt10b* and *Fgf2* supports a model in which WNT10B and FGF2 act upstream to induce *Shh*
306 expression.
307 To identify the cell populations expressing *Wnt10b* and *Fgf2* during normal regeneration,
308 we reanalyzed published single-cell RNA-seq data from a 7 dpa (MB) blastema (Li et al., 2021, Fig.

309 S6). The dataset was reclustered, and clusters were assigned using known markers (*Prrx1* for
310 mesenchyme and *Krt17* for epithelium, Fig. S6A, B). As expected, *Lmx1b*, *Fgf8*, and *Shh* were
311 detected in the mesenchymal cluster (Fig. S6C, F, G). *Fgf2* was also expressed in the mesenchymal
312 cluster (Fig. S6E). In contrast, *Wnt10b* expression was detected in both mesenchymal and epithelial
313 clusters (Fig. S6D). Both *Wnt10b* and *Fgf2* were expressed in only a few cells, consistent with the *in*
314 *situ* hybridization data (Fig. S5A). We then examined the relationships between these genes. *Fgf8*
315 and *Shh* were expressed in both *Lmx1b*-positive and *Lmx1b*-negative cells (Fig. S6H, I), but *Fgf8*
316 and *Shh* themselves were mutually exclusive (Fig. S6M). These expression patterns of *Fgf8*, *Shh*,
317 and *Lmx1b* in the normal blastema are consistent with those observed in ALM blastemas (Fig. 2).
318 For *Wnt10b* and *Fgf2*, their expression did not follow *Lmx1b* expression (Fig. S6J, K), and *Wnt10b*
319 and *Fgf2* themselves were not exclusive (Fig. S6L). Together with the RT-qPCR data (Fig. S5B),
320 these results suggest that *Wnt10b* and *Fgf2* are not exclusively confined to purely dorsal or ventral
321 cells at the single-cell level, even though they show dorsoventral bias when assessed in bulk tissue.
322
323 ***Limb formation without nerve deviation and ventral skin grafting***
324 A previous study demonstrated that a cocktail of BMP2, FGF2, and FGF8 can substitute for nerve
325 deviation in the ALM experiment on the anterior region, suggesting that nerves contribute to
326 blastema induction by supplying these proteins (Makanae et al., 2014). We found that FGF2 can also
327 substitute for ventral tissue in DorBL (Fig. 5), suggesting that FGF2 serves not only as part of the
328 nerve factors in blastema induction but also as the ventral-mediated signal in limb patterning. To
329 investigate whether supplementation with BMP2, FGF2, and FGF8 to the dorsal region could
330 substitute for both nerve deviation and ventral skin grafting, we performed experiments involving
331 gelatin beads soaked in these proteins (Fig. 6). The dorsal or ventral skin was removed at the
332 zeugopod level, and a BMP2+FGF2+FGF8-soaked gelatin bead was grafted at 3 dps without nerve
333 deviation. Blastema induction was observed in both experimental groups (Fig. 6A, B, upper panels).
334 We investigated gene expression patterns in the induced blastemas and found that both *Fgf8* and *Shh*
335 were expressed in blastemas induced at the dorsal site (n=8/8), whereas *Shh* expression was absent
336 in ventral blastemas (n=5/5), although *Fgf8* expression was detected in most cases (n=4/5, Fig. 6C,
337 D, F, G). *Lmx1b* expression patterns corresponded to those observed in DorBL and VentBL (Fig. 6E,
338 H, n=8/8 and 5/5, respectively). Furthermore, limb patterning was observed in the dorsal groups
339 (n=12/20) but not in the ventral groups (n=17/17, Fig. 6A, B, lower panels). These findings
340 demonstrate that a straightforward procedure involving dorsal skin wounding and supplementation
341 with BMP2, FGF2, and FGF8 is sufficient to induce accessory limb formation. This method enabled
342 the induction of an ectopic limb without surgical nerve deviation, but a previous study has shown

that fine nerve ingrowth can still occur when blastemas are induced by a BMP2+FGF2+FGF8-soaked bead (Makanae et al., 2014). These recruited nerves may be functional after blastema induction. Remarkably, this method also enabled the induction of multiple limbs within the same limb. Grafting BMP2+FGF2+FGF8-soaked beads to multiple dorsal sites resulted in the formation of multiple limbs along the proximodistal axis (n=16/35, Fig. 6I–L). Despite careful implantation designed to avoid injuring deep tissues, one sample displayed a fusion of the stylopod with the host humerus—a phenotype associated with deep wounding (Satoh et al., 2010; Makanae et al., 2014). This suggests that contributions from a broader cellular population cannot be excluded. However, because this fusion was not consistently observed, and because ectopic limbs induced at the forearm (zeugopod) level did not exhibit such fusion (n=1/6 for stylopod-level inductions; n=0/10 for zeugopod-level inductions, Fig. 6L1, L2), the data suggest that most ectopic limbs would have developed without substantial ventral-cell contribution. These results refine our understanding of the role of FGF2 in the ALM, particularly its critical function on the dorsal side.

358 ## *Discussion*

359 ### *Dorsal- and ventral-mediated signals are required for the induction of Shh expression*

360 In axolotl limb regeneration, cells derived from all four positional origins—anterior, posterior,
361 dorsal, and ventral—are required for an induced blastema to form a limb. This was confirmed
362 through the ALM experiments (Fig. 1). The gene expression patterns in these ALM blastemas
363 revealed distinct molecular characteristics for each group (Fig. 2). *Fgf8* expression in AntBL and *Shh*
364 expression in PostBL are consistent with a previous report (Nacu et al., 2016). The absence of SHH
365 in AntBL and of FGF8 in PostBL likely accounts for their failure to form limbs. *Lmx1b* expression in
366 the dorsal half of both AntBL and PostBL suggests that both dorsal and ventral tissues co-existed in
367 these blastemas (Fig. 2B, G, Fig. S1A, D). In contrast, DorBL and VentBL exhibited distinct *Lmx1b*
368 expression patterns, suggesting that most cells in DorBL and VentBL are derived from dorsal or
369 ventral origins, respectively (Fig. 2L, Q, Fig. S1G, J). A possible explanation for the lack of *Shh*
370 expression in DorBL and VentBL is that the induction of *Shh* expression may depend on the co-
371 existence of dorsal and ventral cells, although *Fgf8* can be expressed independently of the co-
372 existence of dorsal and ventral cells (Fig. 2M, N, R, S, U, V, Fig. S1H, I, K, L). This idea is
373 supported by the cell-tracing experiment (Fig. 3). In these assays, the posteriorly derived cells
374 expressed *Shh* only when both dorsal and ventral cells were present. These results strongly suggest
375 that the co-existence of dorsal and ventral cells is necessary for inducing *Shh* expression.
376 Consequently, one of the essential roles of the dorsal and ventral cells in limb patterning is to
377 mediate signals required for *Shh* induction in the posterior cells, which facilitates the anteroposterior
378 interaction.

379 Our findings clarify the hierarchical relationship between dorsal- and ventral-mediated
380 signals and anteroposterior interaction. Our data demonstrate that dorsal and ventral cells are
381 essential for inducing *Shh* expression in a regenerating blastema. Furthermore, we showed that
382 DorBL and VentBL, which typically fail to form a limb, could form patterned limbs with ectopic *Shh*
383 expression, even in the absence of dorsal and ventral cell co-existence (Fig. 4). Furthermore, such
384 limbs exhibited dorsally or ventrally symmetric structures (Fig. 4F, G, J–R, Fig. S2C, D),
385 highlighting that dorsoventral patterning depends on the cell origin. Thus, we concluded that dorsal-
386 and ventral-mediated signals are essential for patterned limb formation via inducing *Shh* expression.
387

388 ### *WNT10B and FGF2 as dorsal- and ventral-mediated signals*

389 We identified *Wnt10b* and *Fgf2* as candidate genes encoding the dorsal- and ventral-mediated signals
390 required to induce *Shh* expression, respectively (Fig. 5). Our DEG analysis between DorBL and
391 VentBL revealed higher *Wnt10b* expression in DorBL and higher *Fgf2* expression in VentBL (Fig.

5A, B). *Wnt10b*-electroporation in VentBL and *Fgf2*-electroporation in DorBL induced *Shh* expression and subsequent limb patterning (Fig. 5C–E). *Wnt4* expression was also elevated in DorBL, while *Fgf7* and *Tgfb2* were upregulated in VentBL. However, we did not observe *Shh* induction in the *Fgf7*-electroporated or *Tgfb2*-electroporated DorBL or in the *Wnt4*-electroporated VentBL. FGF7 is known to be capable of inducing the apical ectodermal ridge (AER) in chick limb development (Yonei-Tamura et al., 1999), but little is known about its role in limb regeneration. In newt limb regeneration, KGFR, which acts as an FGF7 receptor, is expressed in the basal layer of the wound epithelium, while FGFR1, which acts as an FGF2 receptor, is primarily expressed in the mesenchyme (Poulin et al., 1993). This differential expression pattern suggests that FGF2 and FGF7 target distinct cell populations, potentially explaining the differences in their ability to induce *Shh* expression. The difference in the ability of *Wnt10b* and *Wnt4* to induce *Shh* expression in VentBL may reflect differences in how these ligands activate downstream WNT signaling programs. WNT10B is a potent activator of the canonical WNT signaling pathway (Bennett et al., 2005), although WNT10B has also been reported to trigger a β-catenin–independent pathway (Lin et al., 2021). Similarly, WNT4 can activate both the canonical WNT signaling pathways and a non-canonical, β-catenin–independent pathway (Li et al., 2013; Li et al., 2019). We also observed *Shh* induction in BIO-treated VentBL, indicating that the canonical WNT signaling pathway regulates *Shh* expression. However, it is uncertain why *Shh* expression was observed in *Wnt10b*-electroporated VentBL, but not in *Wnt4*-electroporated VentBL. One possible explanation is that different WNT ligands can engage the same receptors (Frizzled/LRP6) yet elicit distinct downstream programs, suggesting that such ligand-specific outputs may vary depending on cell context (Voss et al., 2025). Regarding *Tgfb2*, TGF-β signaling has been implicated in blastema induction during salamander limb regeneration (Sader and Roy, 2022; Lévesque et al., 2007). However, little is known about the relationship between TGF-β signaling and *Shh* induction in limb development and regeneration, suggesting that TGF-β signaling does not play a primary role in *Shh* induction. Consistent with this, we did not observe *Shh* induction in the *Tgfb2*-electroporated DorBL, as described above. This suggests that TGFB2 signaling may be involved in dorsoventral regulation independent of *Shh* induction. Taken together, among the candidate genes we identified, WNT10B via the canonical WNT pathway and FGF2 via FGFR1 appear to regulate *Shh* induction and the subsequent patterning process.

WNT signaling may be the key for the dorsal properties in limb formation. It has been reported that canonical WNT/β-catenin signaling plays essential roles in limb regeneration among vertebrates, including axolotls (Kawakami et al., 2006; Lovely et al., 2022). In the present study, we demonstrated that introducing *Wnt10b* or BIO treatment could induce *Shh* expression in VentBL,

426 facilitating limb patterning. In mouse limb development, *Wnt10b* is expressed in the apical
427 ectodermal ridge (AER, Witte et al., 2009), and mutations in *Wnt10b* are associated with Split-
428 Hand/Foot Malformation (Ugur and Tolun, 2008; Al Ghamdi et al., 2020; Bilal et al., 2023).
429 However, there is no evidence suggesting that *Wnt10b* contributes to dorsal specificity during limb
430 development. This raises questions about whether the function of *Wnt10b* is unique to axolotls or
431 whether its orthologs in other species might share functional redundancy with other WNT genes.
432 Further studies are needed to clarify this point. Notably, WNT10B utilizes the canonical Wnt
433 signaling pathway, similar to WNT7A, a well-known WNT family gene critical for dorsoventral
434 limb patterning in amniotes. In amniotes, *Wnt7a* is expressed in the dorsal ectoderm of developing
435 limb buds and induces *Lmx1b* expression in dorsal mesenchyme, thereby establishing dorsal
436 characteristics (Riddle et al., 1995; Cygan et al., 1997; Chen, 2002). In axolotls, dorsal-specific
437 *Wnt7a* expression has not been confirmed. Our RNA-seq analysis showed that there was almost no
438 significant difference in *Wnt7a* expression levels between DorBL and VentBL ($\log_2$ (normalized
439 counts) = 5.97, $\log_2$ (fold change) = -0.810, $p = 0.401$), consistent with previous studies (Shimokawa
440 et al., 2013). Similarly, there was no significant difference in *En1* expression ($\log_2$ (normalized
441 counts) = 0.909, $\log_2$ (fold change) = -1.812, $p = 0.264$). In amniote limb development, *En1* is
442 expressed in the ventral ectoderm, where it restricts *Wnt7a* expression to the dorsal ectoderm and
443 thereby prevents induction of *Lmx1b* in the ventral mesenchyme (Loomis et al., 1996; Logan et al.,
444 1997; Chen and Johnson, 2002). These results suggest that *Wnt7a* does not have a dorsal-specific
445 function, at least in axolotl limb regeneration. While WNT10B could function as a dorsal-mediated
446 signal, WNT10B is unlikely to induce dorsal identity, as ectopic *Lmx1b* expression was not observed
447 in *Wnt10b*-introduced VentBL, which formed double-ventral limbs (Fig. 5F–H). This indicates that
448 *Wnt10b* in axolotl limb regeneration does not simply replace the function of *Wnt7a* in amniote limb
449 development. Nevertheless, the involvement of canonical WNT signaling in dorsal function and limb
450 morphogenesis remains an important area for further investigation.
451 We identified FGF2 as the ventral-mediated signal, which plays a crucial role in the limb
452 patterning process during axolotl limb regeneration. This aligns with previous studies showing that
453 *Fgf2* expression correlates with limb regeneration in salamanders (Giampaoli et al., 2003). *Fgf2*
454 expression was relatively high in VentBL, and *Fgf2*-introduced DorBL formed patterned limbs (Fig.
455 5). These results indicate that *Fgf2* overexpression can substitute for the presence of ventral cells in
456 the limb patterning process. It is noteworthy that FGF2 application does not appear to induce ventral
457 identity, as the limbs formed from *Fgf2*-introduced DorBL exhibited dorsally symmetric limb
458 structures. The use of FGF signaling as a ventral-mediated output downstream of dorsoventral
459 identity has not been documented in other species examined to date. Whether this represents an

axolotl-specific regulatory mechanism or a broader function of FGF signaling in limb morphogenesis remains to be determined.

Our findings suggest that although WNT10B and FGF2 act as dorsal- and ventral-mediated signals, they do not alter dorsal or ventral identity itself. In amniote limb development, WNT7A and EN1 regulate dorsoventral identity through *Lmx1b* expression. In contrast, in axolotls, *Wnt10b*-electroporation in VentBL or *Fgf2*-electroporation in DorBL did not affect the expression patterns of *Lmx1b* (Fig. 5C). Moreover, the limbs formed from such DorBL and VentBL exhibited dorsally or ventrally symmetric structures (Fig. 5H–J, Fig. S4). These findings suggest that dorsoventral identities in axolotls are not affected by *Wnt10b* or *Fgf2* overexpression. We previously reported that the expression patterns of *Lmx1b* in axolotl limb regeneration are likely to depend on the positional origins of cells (Iwata et al., 2020; Yamamoto et al., 2022). The identities of cells along the dorsoventral axis may be controlled by their positional memory and determined before the initiation of limb regeneration.

The present study revealed that the dorsal- and ventral-mediated signals WNT10B and FGF2 regulate *Shh* expression during limb patterning in axolotls. These findings highlight a degree of conservation between axolotl limb regeneration and amniote limb development. In amniote limb development, FGF and WNT signaling pathways are key regulators of *Shh* expression. In developing amniote limb buds, *Fgf2* is expressed in the ectoderm, including the AER, and in adjacent mesoderm, and promotes distal outgrowth. FGFs, including FGF2, supplied from the AER are known to maintain *Shh* expression (Laufer et al., 1994; Niswander et al., 1994; Yang and Niswander, 1995; Li et al., 1996). Similarly, WNT7A regulates *Shh* expression in amniote limb development, and loss of WNT7A function results in reduced *Shh* expression in the zone of polarizing activity (ZPA) and the deletion of posterior structures (Parr and McMahon, 1995). Thus, our findings provide new insight into both conserved and divergent aspects of dorsal- and ventral-mediated signaling in the regulation of *Shh* expression, thereby furthering our understanding of limb morphogenesis.

In this study, RNA-seq analysis of ALM blastemas induced on the dorsal or ventral side listed *Wnt10b* and *Fgf2* as genes that are more highly expressed in DorBL and VentBL, respectively. In the ALM context, *Wnt10b* or *Fgf2* overexpression was sufficient to substitute for dorsal or ventral tissues, respectively, and to drive *Shh* induction and subsequent limb patterning even in the absence of those tissues (Fig. 5). However, in amputation-induced blastemas during normal regeneration, *in situ* hybridization did not reveal clear expression patterns for *Wnt10b* or *Fgf2* (Fig. S5A), and reanalysis of single-cell RNA-seq from the regenerating blastema (Li et al., 2021) showed that their expression did not strictly follow *Lmx1b* expression (Fig. S6J, K). By contrast, and consistent with our bulk RNA-seq results, RT-qPCR of manually microdissected dorsal and ventral halves of

494 regenerating blastemas showed that *Wnt10b* and *Fgf2* were expressed at significantly higher levels in
495 the dorsal and ventral halves, respectively (Fig. S5B). These results suggest that *Wnt10b* expression
496 and *Fgf2* expression are mediated by dorsal and ventral cells, respectively, but their expression is not
497 restricted to dorsal or ventral cells. Our results on *Wnt10b*-electroporated VentBL and *Fgf2*-
498 electroporated DorBL suggest that both activation of WNT10B or FGF2 is required for *Shh*
499 induction and proceed with limb patterning. To fully understand axolotl limb regeneration, it will be
500 important to determine how *Wnt10b* and *Fgf2* expression is regulated, how their downstream
501 programs are deployed, and how dorsal and ventral cells respond to these signals in future studies.
502
503 ***The dorsoventral-mediated Shh induction mechanism***
504 In the present study, we found the importance of the co-presence of cells carrying the
505 anterior, posterior, dorsal, and ventral identity for successful axolotl limb patterning (Fig. 7). In our
506 proposed model, following amputation, nerves first trigger blastema induction by secreting nerve
507 factors, such as BMPs and FGFs (Makanae et al., 2014, Satoh et al., 2016). These nerve factors
508 stimulate connective tissue cells, including dermal cells, to generate multipotent mesenchymal
509 blastemal cells (Muneoka et al., 1986; Kragl et al., 2009; Hirata et al., 2010; Gerber et al., 2018).
510 Within the induced blastema, *Wnt10b* and *Fgf2* expression are mediated by the dorsal and ventral
511 cells, respectively. In the next phase, the co-existence of WNT10B and FGF2 signaling induces *Shh*
512 expression in the posterior region of the blastema. During this phase, *Fgf8* is expressed in the
513 anterior mesenchyme independently of the co-existence of dorsal and ventral cells (Fig. 7A). These
514 expression patterns of *Wnt10b*, *Fgf2*, *Shh*, and *Fgf8* may be mediated by the positional memory of
515 cells (Otsuki et al., 2021). In the subsequent phase, the anteroposterior interaction, mediated by
516 FGF8 and SHH, supports distal outgrowth to form a limb. This model explains previous
517 observations in studies on double-half limbs and ALM blastemas (AntBL, PostBL, DorBL, and
518 VentBL), which typically fail to form a limb. In blastemas induced from double-anterior and double-
519 posterior limbs, or AntBL (Fig. 7B) and PostBL (Fig. 7C), SHH or FGF8 proteins are likely absent
520 due to the lack of posteriorly or anteriorly derived cells, respectively. Similarly, in blastemas induced
521 by amputating double-dorsal and double-ventral limbs, or DorBL (Fig. 7D) and VentBL (Fig. 7E),
522 FGF2 or WNT10B proteins are likely absent or insufficient because of the lack of ventrally or
523 dorsally derived cells, respectively. This results in the absence of SHH, even if posteriorly derived
524 cells are present. In all these cases, the absence of either FGF8 or SHH disrupts the anteroposterior
525 interaction, leading to failure in limb patterning. We conclude that the requirement for cells derived
526 from all four positional origins is underpinned by this model. In this model, dorsal- and ventral-
527 mediated signals activate the posterior SHH, enabling mutual interaction with the anterior FGF8.

This interplay ensures proper anteroposterior interaction and complete limb patterning. Our findings contribute to understanding how the integration of four positional identities—dorsal, ventral, anterior, and posterior—drives proper limb patterning during axolotl limb regeneration.

Materials and Methods

Animal procedures

Axolotls between 4 and 15 cm from snout to tail tip were housed in tap water at 22°C. Both forelimbs and hind limbs were used for surgical procedures without distinction. Transgenic axolotls were obtained from the Ambystoma Genetic Stock Center (http://www.ambystoma.org/genetic-stock-center). Animals were anesthetized in 0.1% MS222 (Sigma-Aldrich) solution before surgical procedures.

In the ALM experiments, skin was peeled from the anterior, posterior, dorsal, or ventral side of a limb at the stylopod level, so that the skin of the opposite side was not injured. Thus, the size of the injured area depended on the limb size. Then, thick bundles of nerve trunks running the center of a limb was deviated the injured region. For the cell-tracing experiment, a piece of posterior half of the dorsal or ventral skin was obtained from GFP-expressing transgenic animals and grafted to the ALM region.

Protein-soaked beads for grafting were prepared as previously described (Makanae et al., 2014; Kashimoto et al., 2023). In brief, air-dried gelatin beads were allowed to swell in stock solution (1 μg/μL) prepared following the manufacturer's instructions. Equal amounts of proteins were used when formulating the combination protein mixture. Beads were soaked in the mixture of proteins (Bmp2 [mouse], Fgf2 [mouse], and Fgf8 [human/mouse]; R&D Systems) overnight at 4°C. For control experiments, gelatin beads were soaked in DDW. Before grafting, dorsal or ventral skin was peeled because full-thickness skin inhibits limb regeneration (Thornton, 1962; Mescher, 1976; Tsai, 2020). The beads were grafted under the wounded epidermis at 3 dps. The limbs were fixed 10 days after grafting. The details of grafting procedures are as previously described (Makanae et al., 2014; Kashimoto et al., 2023).

To analyze skeletal patterns, induced limbs were stained with alcian blue and alizarin red. Samples were fixed in 100% ethanol for 1 day at room temperature, then stained with Alcian blue solution (Wako, pH 2.0) in 20% acetic acid (Nacalai Tesque) with 80% ethanol solution at 37°C overnight. Then, samples were washed in tap water several times and fixed in 10% Formaldehyde Neutral Buffer Solution (Nacalai Tesque) for 1 day. Samples were then stained with Alizarin red S (Nacalai Tesque) in the solution (4% KOH:10% Formaldehyde Neutral Buffer Solution = 2:3) at room temperature for 1 day. Finally, samples were placed in graded glycerol with 4% KOH for clearing.

For BIO treatment, 10 mM stock solution of 6-bromoindirubin-3-oxime (BIO, Selleck, S7198) dissolved in DMSO was stored in the dark at 4°C. Axolotls soon after surgery were raised in tap water with BIO solution (experimental) or with the same amount of solvent, DMSO (control), until 14 dps for RT-qPCR and 30 dps for phenotype analysis. The containers including water and axolotls were kept in the dark during BIO or DMSO treatment. For BIO treatment, axolotls between

568 4 and 5 cm from snout to tail tip were used.
569
570 ***Sectioning and histological staining***
571 Samples were fixed in 4% PFA/PBS overnight at room temperature before sectioning. The fixed
572 samples were embedded in O.C.T. compound (Sakura) following 30% sucrose/PBS treatment for
573 approximately 12 h at 4°C. Frozen sections of 14 μm thickness were prepared using Leica CM1850
574 (Nussloch). The sections were well dried under an air dryer and kept at -80°C until use.
575 Standard hematoxylin and eosin (HE) staining and Masson's trichrome staining were used
576 for histological analysis. To visualize cartilage formation, Alcian blue staining was performed before
577 HE staining. In brief, sections were washed in tap water several times to remove the O.C.T.
578 compound. Then, the sections were stained with Alcian blue (Wako, pH 2.0), and then HE staining
579 was performed. Trichrome stain (Masson) kit (Sigma, HT15-1KT) was used for trichrome staining.
580 The stained sections were mounted using Softmount (Wako).
581
582 ***In situ hybridization***
583 *In situ* hybridization was performed as described previously (Yamamoto et al., 2022). For probe
584 synthesis, target genes cloned on pTAC-2 plasmid (BioDynamics Lab Inc.) were amplified by PCR
585 using M13 primers. PCR fragments were purified and used as an RNA probe template. RNA probe
586 synthesis was performed with Sp6 or T7 RNA polymerase (Takara) for 3 h, and RNA was
587 hydrolyzed, depending on the length of targets. The sections were washed in PBT to remove the
588 O.C.T. compound, treated with proteinase K (10 μg/mL) (Invitrogen)/PBT for 20 min at room
589 temperature, washed in PBT, treated with 4% PFA/PBS for 20 min at room temperature, washed in
590 PBT, and then probes were hybridized at 62.5°C for approximately 18 h. The sections were washed
591 in wash buffer 1 (formamide:H_2O:20× SSC [3M NaCl:0.3M sodium citrate, pH 5.0] = 2:1:1), and
592 then in wash buffer 2 (formamide:H_2O:20× SSC = 5:1:4). The samples were then incubated with
593 anti-digoxigenin-AP Fab fragments (Sigma-Aldrich, 1/1000) for 2 h at room temperature. Samples
594 were stained with BCIP (Nacalai Tesque) and NBT (Nacalai Tesque) in alkaline phosphatase buffer
595 (0.1M NaCl, 0.1M Tris-HCl [pH9.5], 0.1% Tween20) for 18 h at room temperature after washing in
596 TBST.
597
598 ***Immunofluorescence***
599 Immunofluorescence on sections was carried out based on a previous report (Yamamoto et al.,
600 2022). The antibodies were as follows: anti-GFP (MBL, #598, 1/500), anti-acetylated alpha tubulin
601 (Santa Cruz, #sc-23950, 1/1000), anti-mouse IgG Alexa 488 (Invitrogen, #A11017, 1/1000), anti-
602 rabbit IgG Alexa 488 (Invitrogen, #A21206, 1/500). Nuclei were stained with Hoechst (Nacalai

603 Tesque), and images were captured using an Olympus BX51 system.
604
605 ***RNA-Seq analysis***
606 Total RNA was extracted from DorBL and VentBL at 10 dps using TriPure reagent (Roche),
607 following the manufacturer's instructions. Three biological replicates were prepared for both
608 samples. 150 bp paired-end RNA-seq reads were obtained under contract to Rhelixa (Tokyo, Japan),
609 using Illumina Nova Seq 6000 and SMART-Seq HT Plus Kit (#R400449). RNA-seq data were
610 analyzed on Galaxy (https://usegalaxy.eu/root) as follows. Sequence reads were trimmed and the
611 quality was filtered by Trimmomatic v0.39 (Bolger et al., 2014) with the following parameters
612 (LEADING:20, TRAILING:20, SLIDINGWINDOW:4:15, MINLEN:36). Axolotl genome data
613 (AmexG_v6.0-DD) and annotation data (AmexT_v47-AmexG_v6.0-DD.gtf) were obtained from
614 AXOLOTL-OMICS (https://www.axolotl-omics.org/) (Schloissnig et al., 2021). Mapping to the
615 Axolotl genome (AmexG_v6.0-DD) was performed with HISAT2 v2.2.1 (Kim et al., 2015). Count
616 data were obtained with featureCounts v2.0.8 (Liao et al., 2013) on the basis of the Axolotl gene
617 model (AmexT_v47-AmexG_v6.0-DD.gtf). DEGs were identified with DESeq2 v2.11.40.8 (Love et
618 al., 2014) ($p < 0.05$). Among identified DEGs (DorBL > VentBL; 762 genes, VentBL > DorBL; 513
619 genes), genes annotated as "intercellular signaling molecule" were explored on PANTHER
620 (https://www.pantherdb.org/) (Thomas et al., 2003), and 21 genes (DorBL > VentBL; 5 genes,
621 VentBL > DorBL; 16 genes) were identified as candidate genes of dorsal- and ventral-mediated
622 signals, as shown below:
623
624 DorBL > VentBL:
625 WNT4 (AMEX60DD052091), WNT10B (AMEX60DD029981), SEMA3A (AMEX60DD023165),
626 LECT2 (AMEX60DD041044), ANGPTL5 (AMEX60DD049512).
627
628 VentBL > DorBL:
629 FCN1 (AMEX60DD050926), CXCL14 (AMEX60DD028973), DNER (AMEX60DD002010),
630 FGF7 (AMEX60DD003767), CXCL12 (AMEX60DD052412), CXCL8 (AMEX60DD044133),
631 SEMA6A (AMEX60DD042813), ANGPTL2 (AMEX60DD050490), ANGPTL6
632 (AMEX60DD031854), FGL2 (AMEX60DD006387), VWDE (AMEX60DD022491), TGFB2
633 (AMEX60DD036126), FGF2 (AMEX60DD044865), EFNA4 (AMEX60DD014882), EFNA3
634 (AMEX60DD014867), ANGPTL1 (AMEX60DD018261).
635
636 ***Cloning candidate genes and preparation of construct vectors for overexpression***
637 Among the identified candidate genes, we focused on *Wnt10b*, *Wnt4*, *Fgf2*, *Fgf7*, and *Tgfb2*. We

638 cloned these genes in pTAC-2 plasmids from cDNA obtained from blastemas. The following primers
639 were used:
640
641 Wnt10b Fwd:ATGGCCCACAGCTCACCCTCCGACACC
642 Wnt10b Rev:TCACTTGCACACATTCACCCATTCTGTG
643 Wnt4 Fwd:ATGGATGCTCACGAAAGCAGCGTATATC
644 Wnt4 Rev:TCACCGGCAGGTGTGCATTTCTACCAC
645 Fgf2 Fwd:ATGGCGGCGGGGAGCATCACCACCTTGC
646 Fgf2 Rev:TCAACTCTTGGCCGACATGGGAAGGAAAAG
647 Fgf7 Fwd:ATGCGCAGATGGGTGCTAGCTTGGATC
648 Fgf7 Rev:TCATGTGTTATTGGATATACGCATTGGA
649 Tgfb2 Fwd:ATGAGATTACAATTACTGAGAAAAAAAAATG
650 Tgfb2 Rev:TTAGCTGCACTTGCAAGATTTTACAATCA
651
652 We then inserted these genes to p2a-AcGFP-pCS2 vectors with In-Fusion® HD Cloning Kit
653 (Clontech). The following primers were used for PCR before In-Fusion reaction:
654
655 pCS2 inverse Fwd:GCTACTAACTTCAGCCTGCTGAAGCAGG
656 pCS2 inverse Rev:CATCGATGGGATCCTGCAAAAAGAACAAGTAGCTT
657 Wnt10b Fwd:AGGATCCCATCGATGGCCCACAGCTCACCCTCCGA
658 Wnt10b Rev:GCTGAAGTTAGTAGCCTTGCACACATTCACCCA
659 Wnt4 Fwd:AGGATCCCATCGATGGATGCTCACGAAAGCAGCG
660 Wnt4 Rev:GCTGAAGTTAGTAGCCCGGCAGGTGTGCATTTCTA
661 Fgf2 Fwd:AGGATCCCATCGATGGCGGCGGGGAGCATCACCA
662 Fgf2 Rev:GCTGAAGTTAGTAGCACTCTTGGCCGACATGGGAA
663 Fgf7 Fwd:AGGATCCCATCGATGCGCAGATGGGTGCTAGCTTG
664 Fgf7 Rev:GCTGAAGTTAGTAGCTGTGTTATTGGATATACGCA
665 Tgfb2 Fwd:AGGATCCCATCGATGAGATTACAATTACTGAGAAA
666 Tgfb2 Rev:GCTGAAGTTAGTAGCGCTGCACTTGCAAGATTTTA
667
668 Finally, the following DNA constructs were obtained; *Wnt10b*-p2a-GFP (pCS2), *Wnt4*-p2a-GFP
669 (pCS2), *Fgf2*-p2a-GFP (pCS2), *Fgf7*-p2a-GFP (pCS2), and *Tgfb2*-p2a-GFP (pCS2).
670
671 ***Electroporation***
672 Each DNA construct was injected directly into the target region. Immediately after injection, electric
673 pulses were applied (20 V, 50 ms pulse length, 950 ms interval, 10 times) with NEPA21(Nepa gene).

674 The injected DNA constructs were as follows: pCS2-AcGFP, pCS2-*Shh*-p2a-AcGFP, *Wnt10b*-p2a-
675 GFP (pCS2), *Wnt4*-p2a-GFP (pCS2), *Fgf2*-p2a-GFP (pCS2), *Fgf7*-p2a-GFP (pCS2), and *Tgfb2*-p2a-
676 GFP (pCS2). All plasmids were purified using a Genopure Maxi kit (Roche). Electroporation was
677 performed at -3, 4, and 7 dps and samples were fixed at 10 dps for *in situ* hybridization. To analyze
678 the phenotype of 90 dps samples, electroporation was performed at -3, 4, 7, 10, 15, 20, 25, and 30
679 dps.
680
681 ***qRT-PCR***
682 The procedures of qRT-PCR were previously described (Yamamoto et al., 2022). In brief, RT was
683 performed using Prime Script II (Takara), and RT-qPCR was performed using KAPA SYBR FAST
684 qPCR Master Mix (Kapa Biosystems) and StepOne (ThermoFisher Scientific). Primers were as
685 follows:
686
687 Ef-1α Fwd: AACATCGTGGTCATCGGCCAT
688 Ef-1α Rev: GGAGGTGCCAGTGATCATGTT
689 Shh Fwd: GCTCTGTGAAAGCAGAGAACTCG
690 Shh Rev: CGCTCCGTCTCTATCACGTAGAA
691 Axin2 Fwd: GGCACTGACTTATCCCCAGG
692 Axin2 Rev: GCATCATTGGCTGTCAACGG
693 Lef1 Fwd: CTACACCGAGATCAGCCACC
694 Lef1 Rev: GCTGTGGTAGGAGTTGTGGG
695 Lmx1b Fwd: CTGGTCCATGGCTACGATCT
696 Lmx1b Rev: TTAGCAGCAGAAACGGGACT
697 Wnt10b Fwd: CAGAAGAGACCCAGGTGCAG
698 Wnt10b Rev: CGAAGGCCCAAGATGTCTGT
699 Fgf2 Fwd: TCTTCCTTCGCATCAACCCC
700 Fgf2 Rev: TTTCATTGCCATCAACCGCC
701
702 RNA for Fig. S3E was prepared from 1μM BIO- or DMSO-treated VentBL at 14 dps. *Ef-1α* was
703 used as the internal control.
704
705 ***Pixel classification and calculating symmetry scores***
706 A machine learning-based method was applied for pixel classification using ilastik software
707 (downloaded on https://www.ilastik.org/). The details and workflows were previously described
708 (Berg et al., 2019). Each pixel in the images was classified into five classes. The regions of the
709 background (Class 1), cartilage (Class 2), muscle (Class 3), other connective tissue (Class 4), and

epidermis (Class 5) were annotated for training data. Using these annotated regions as references, pixels were automatically classified into the respective classes. In this process, the same training data were used for images obtained from the same limb. Then, symmetry scores were calculated for each class individually and for the combined set of all classes. In this process, the external shape of the section, which could bend randomly during sample fixation process, would affect the symmetry scores if the entire region were used. To focus on the symmetry of the anatomical patterns, images with 400 μm width were prepared (Fig. 4L, 5E, F). The symmetry scores of pixel-classified images were calculated using python. First, the center of the dorsal end and ventral end was set as the axis of symmetry. Then, one side of the image was flipped. Next, color masks were generated for both sides of the image. These masks identified pixels that matched the specified color. Pixels were considered to match if their RGB values were within the given tolerance range for all three channels. In pixel comparison, the masks for one side and the other side were compared to calculate the following pixels:

Matching pixels: The number of pixels that match in both sides for the specified color.
Total pixels: The total number of pixels matching the color in either side.

The symmetry scores were computed as (Number of Matching Pixels)/(Total Pixels in Both Sides). The scores were obtained from 12 areas of each group. For statistical analysis, a two-tailed a two-tailed Welch's *t*-test was used. In this analysis, each group was compared to the intact limb group because the intact limb should be set as a typical asymmetrical structure.

Reanalyzing single-cell data

We reanalyzed published single-cell RNA-seq data from a 7 dpa (MB) blastema (Li et al., 2021, Fig. S6). We constructed a transcriptome index for axolotl from the available genome assembly and gene annotation (AmexG_v6.0-DD genome and AmexT_v47-AmexG_v6.0-DD annotation, Schloissnig et al., 2021). The transcript set was used to build a salmon index with default k-mer length (31), and without decoy sequences, and gene-level UMI counts were generated using the Alevin module of salmon, which performs lightweight (quasi-)mapping of reads directly to the transcriptome index (Patro et al., 2017; Srivastava et al., 2019). The mapping was done on Galaxy (https://usegalaxy.eu). This procedure yielded a whitelist of 8,925 barcodes, corresponding to putative cells, and produced a per-cell by per-gene UMI count matrix. According to the Alevin summary output, 77.4% of reads aligned to the indexed axolotl transcriptome after barcode correction and UMI deduplication. The resulting count matrix was exported in Matrix Exchange (MEX) format (matrix.mtx, barcodes.tsv,

features.tsv).

The data were then imported into R (RStudio environment) as a Seurat object, a data structure for scRNA seq data (Hao et al., 2021). Cells were filtered based on standard quality-control metrics, excluding droplets with extremely low gene complexity, extremely high total UMI counts, or unusually high mitochondrial or ribosomal RNA content. For normalization and integration of cells into a shared space, counts were log-normalized using Seurat's NormalizeData (default LogNormalize method with a scale factor of 10,000), and highly variable genes (HVGs) were identified using FindVariableFeatures (vst method; 2,000 features). The data were scaled with ScaleData, and principal component analysis (PCA) was performed on the HVGs (RunPCA, 50 components). The first 30 principal components were used to construct a nearest-neighbor graph (FindNeighbors) and to perform community detection–based clustering (FindClusters, resolution = 0.3). The same set of PCs (dims 1:30) was also used for nonlinear dimensionality reduction by UMAP (RunUMAP). Gene expression patterns were visualized using FeaturePlot with order = TRUE so that high-expressing cells are drawn on top of low- or non-expressing cells. We also generated two-gene "co-expression" maps by classifying cells as expressing gene A only, gene B only, both, or neither, and overlaying these classes on the UMAP using DimPlot.

Author contributions

Conceptualization: S.Y., A.S.; Methodology: S.Y., M.H., A.S; Validation: S.Y.; Formal analysis: S.Y.; Investigation: S.Y.; Resources: S.Y., S.F., A.O., A.S.; Data curation: S.Y.; Writing - original draft: S.Y.; Writing - review & editing: S.Y., S.F., A.O., M.H., A.S.; Visualization: S.Y., A.S.; Supervision: A.S.; Project administration: A.S.; Funding acquisition: A.S., S.Y.

Data availability

RNA-seq FASTQ files have been deposited in the DNA Data Bank of Japan (DDBJ; https://www.ddbj.nig.ac.jp/) under BioProject accession PRJDB38065.

Acknowledgments

We are grateful to R. Iwata and T. Satoh for supporting office work and animal housing. Animals were obtained through Hiroshima University Amphibian Research Center. This work is supported by the Japan Society for the Promotion of Science KAKENHI grant-in-aid for scientific research (B) (20H03264 and 24K02034 to A.S.) and by a Grant-in-Aid for Japan Society for the Promotion of Science fellows (24KJ1718 to S.Y.).

Figure Legends

Figure 1. ALM experiments at the four orientations.

(A) Schematic image of anatomy at the stylopod level of axolotl limb. HE staining (bright field) and acetylated alpha tubulin, visualized by immunofluorescence (green, dark field), are shown in the right panels. Black and white arrows, respectively, indicate major blood vessels and nerves. H: *humerus*, AHL: *Anconaeus humeralis lateralis*, HAB: *Humeroantebrachialis*, CBL: *Coracobrachialis longus*. (B–I) Blastemas induced at the anterior, posterior, dorsal, or ventral region by skin wounding plus nerve deviation without (B–E) or with (F–I) skin grafting from the opposite side of the limb. (F–I) Limb patterning was observed (n=8/9 for F, 4/7 for G, 7/14 for H, and 7/11 for I, see Table 1 for more detail). Images were captured at 10 and 60 dps. Scale bar = 3 mm.

Figure 2. Gene expression patterns of the ALM-induced blastemas.

Sections of anteriorly (A–D), posteriorly (F–I), dorsally (K–N), or ventrally (P–S) induced blastemas at 10 dps. Acetylated alpha tubulin (A–P) was visualized by immunofluorescence. Expression of *Lmx1b* (B–Q), *Fgf8* (C–R), and *Shh* (D–S) in the regions indicated by white boxes in (A–P) was visualized by *in situ* hybridization. Images of the entire blastema are provided in Fig. S1. *Fgf8* expression was observed in AntBL (C), DorBL (M), and VentBL (R) (n=4/5, 4/6, and 4/6, respectively. *Shh* expression was observed in PostBL (I) (n=5/5). In each case, these expression patterns of *Fgf8* and *Shh* were focal and only a few cells expressed *Fgf8* or *Shh*. Black and white arrowheads indicate the signals of *Fgf8* and *Shh* expression, respectively. The dotted line indicates the epithelial-mesenchyme border. (E–T) Schematic images of gene expression patterns. (U, V) Quantitative analysis of *Fgf8* and *Shh* expression in ALM blastemas (n=5 for all groups). n.s.; no significant difference, $*p<0.05$, $**p<0.005$ (two-tailed Welch's *t*-test). Scale bar in (A) = 700 μm.

Figure 3. Co-existence of dorsal and ventral cells induces Shh expression.

(A) Experimental scheme. Posterior half of dorsal (PD_{gfp}) or ventral (PV_{gfp}) GFP-expressing skin was grafted on VentBL (VentBL+PD_{gfp}; C, D / VentBL+PV_{gfp}; G, H), or DorBL (DorBL+PD_{gfp}; E, F / DorBL+PV_{gfp}; I, J) region. (B) Induced blastemas at 10 dps; images of bright and dark fields are merged. (C–J) Dark and bright fields of the same sections of induced blastemas at 10 dps. Red boxes in (C–I) indicate the corresponding regions of lower images. Expression of *Shh* and *Lmx1b* were visualized by *in situ* hybridization. GFP signals were visualized by immunofluorescence. Arrowheads indicate the cells expressing *Shh*. *Shh* expression was observed in VentBL+PD_{gfp} (C) and DorBL+PV_{gfp} (I) (n=4/6 and 3/6, respectively), but not in DorBL+PD_{gfp} (E) and VentBL+PV_{gfp} (G) (n=6/6 and 7/7, respectively). The dotted line indicates the epithelial-mesenchyme border. For all samples, we collected serial sections spanning the entire blastema. For blastemas in which *Shh* expression was observed, we present representative sections showing the signal. For blastemas

814 without detectable *Shh* expression, we present a section from the central region that contains GFP-
815 positive cells. Scale bar = 3 mm (B) and 700 μm (C).
816
817 ***Figure 4. Limb formation without the co-existence of dorsal and ventral cells by Shh***
818 ***overexpresion.***
819 (A) Experimental scheme. *Shh*-p2A-GFP- or GFP-containing pCS2 vector was electroporated (EP)
820 into AntBL, DorBL, and VentBL. (B) Induced blastemas at 14 dps; images of bright and dark
821 fields are merged. (C–G) Phenotypes at 90 dps. Limb patterning was observed in (E–G) (n=10/19,
822 6/18, and 8/14, respectively). (H–K) Histological analysis of intact and induced limbs. Standard
823 Masson's trichrome staining was performed on the transverse sections. The dotted boxes indicate the
824 regions shown in (L). (L) Upper panels: analyzed regions for calculating symmetry scores. Lower
825 panels: images after pixel classification by machine learning. (M–R) Symmetry scores of each class.
826 Scores obtained from the same limb are plotted at the same x-coordinates. n.s.; no significant
827 difference, $*p<0.05$, $**p<0.005$ (two-tailed Welch's *t*-test). Scale bar = 2 mm (B), 4 mm (C–G), and
828 1 mm (H–K).
829
830 ***Figure 5. Identification of candidate molecules of the dorsal- and ventral-mediated signals.***
831 RNA-Seq was performed on DorBL and VentBL at 10 dps. (A) MA plot of the result. (B) List of
832 DEGs annotated as "intercellular signaling molecules." (C) Bright and dark fields of sections of
833 DorBL and VentBL at 10 dps with candidate genes introduced. Expression of *Shh* and *Lmx1b* was
834 visualized by *in situ* hybridization, and GFP signals were visualized by immunofluorescence.
835 Arrowheads indicate the cells expressing *Shh*. The white boxes indicate the regions of the lower
836 panels. Images of dark and bright fields of *Shh* are obtained from the same section. For samples with
837 detectable *Shh* expression, the window was placed in the region where the signal was observed, and
838 for conditions without detectable *Shh* expression, the window was positioned in a comparable region
839 containing GFP-positive cells. *Shh* expression was observed in *Wnt10b*-electroporated VentBL
840 (n=4/5) and *Fgf2*-electroporated DorBL (n=5/7), but not in *Wnt10b*-electroporated DorBL (n=6/6),
841 *Fgf2*-electroporated VentBL (n=5/5), *Fgf7*-electroporated DorBL (n=5/5), *Tgfb2*-electroporated
842 DorBL (n=5/5), or in *Wnt4*-electroporated VentBL (n=6/6). (D, E) Quantitative analysis of *Shh*
843 expression in *Fgf2*- or GFP-electroporated DorBL and *Wnt10b*- or GFP-electroporated VentBL (n=7
844 for both). In each case, *Fgf2* or *Wnt10b* was electroporated into the DorBL or VentBL induced in the
845 left limb, and GFP was electroporated into the contralateral right limb of the same animal. (F, G)
846 Quantitative analysis of *Axin2* and *Lef1* expression in *Wnt10b*- or GFP-electroporated VentBL (n=7
847 for both). (H, I) The limbs formed from VentBL with *Wnt10b* and DorBL with *Fgf2* at 90 dps.
848 Histological analysis and pixel classification was performed in the same way as in Fig. 4. The dotted

849 boxes indicate the regions shown in the right panels. (J) Symmetry scores of each class. Scores
850 obtained from the same limb are plotted at the same x-coordinates. The plots of "int" are the same
851 plots as in Fig. 4. n.s.; no significant difference, *p<0.05, **p<0.005 (two-tailed paired t-test for D–
852 G, and two-tailed Welch's t-test for J). Scale bar = 700 μm (C), 4 mm (H, I, upper panels), 1 mm (H,
853 I, lower panels).
854
855 ***Figure 6. Limb formation at the dorsal region by BMP2+FGF2+FGF8 supplementation.***
856 (A, B) 14 and 60 dps phenotypes of BMP2+FGF2+FGF8 supplementation by bead grafting at the
857 dorsal (A) or ventral (B) region. Neither nerve deviation nor skin grafting was performed. Limb
858 patterning was observed in the dorsa group (A) (n=12/20) but not in the ventral group (B) (n = 0/17).
859 (C–H) Expression patterns of *Fgf8*, *Shh* and *Lmx1b* of induced blastemas at 10 dps. Gene expression
860 was visualized by *in situ* hybridization. The dotted line indicates the external shape of the blastema.
861 *Fgf8* expression was detected in both dorsal and ventral groups (n=8/8 for C and 5/5 for F), whereas
862 *Shh* expression was detected only in the dorsal group (D) (n=8/8) and not in the ventral group (G)
863 (n= 0/5). (I–J) Phenotype obtained by BMP2+FGF2+FGF8 supplementation to two dorsal regions of
864 an identical limb. (K, L) Phenotype obtained by BMP2+FGF2+FGF8 supplementation to five dorsal
865 regions of an identical limb (n=16/35). Scale bar = 3 mm (B), 700 μm (H), 2 cm (J), 1 cm (K, L).
866
867 ***Figure 7. The dorsoventral-mediated Shh induction mechanism.***
868 Schematic images of a normal blastema (A), AntBL (B), PostBL (C), DorBL (D), and VentBL (E).
869 Green, red, blue, and yellow boxes within the blastema represent cells derived from anterior,
870 posterior, dorsal, and ventral regions, respectively. Colored arrows indicate the presence of the
871 corresponding signals mediated by these cells. In this model, limb patterning requires both FGF8 and
872 SHH, and *Shh* expression in posteriorly derived cells is induced by the co-existence of WNT10B and
873 FGF2.
874
875 ***Figure S1. Gene expression patterns across the entire ALM-induced blastemas.***
876 Sections of ALM blastemas induced at the anterior (A–C), posterior (D–F), dorsal (G–I), or ventral
877 (J–L) region at 10 dps. *Lmx1b* (A, D, G, J), *Fgf8* (B, E, H, K), and *Shh* (C, F, I, L) expression was
878 detected by *in situ* hybridization. These panels show the full blastema regions corresponding to the
879 higher-magnification views in Fig. 2. Scale bar = 700 μm (A).
880
881 ***Figure S2. Histological analysis of intact limbs and limbs induced by Shh electroporation.***
882 (A–D) Transverse sections taken at multiple levels along the proximodistal axis from an intact limb

883 and from the limbs shown in Fig. 4. Sections from limbs induced from DorBL and VentBL exhibit
884 dorsoventrally symmetric internal structures, whereas intact limbs and limbs induced from AntBL do
885 not. Scale bar = 1 mm.
886
887 ***Figure S3. Limb patterning from BIO-treated VentBL.***
888 (A, C) VentBL treated with 1μM BIO (C) or DMSO (A) at 90 dps. (E) Quantitative analysis of *Shh*
889 expression in VentBL treated with 1μM BIO and with DMSO. RNA was prepared from 4 identical
890 VentBL for both. Technological replicates are plotted in the same color. (C–D) Histological analysis
891 and pixel classification was performed in the same way as in Fig. 4. The dotted boxes indicate the
892 regions shown in (D). (E) Symmetry scores of each class. Scores obtained from the same limb are
893 plotted at the same x-coordinates. The plots of "int" are the same plots as in Fig. 4. n.s.; no
894 significant difference, *p<0.05, **p<0.005. Scale bar = 4 mm (B), 1 cm (C).
895
896 ***Figure S4. Histological analysis of limbs induced by Fgf2 or Wnt10b electroporation.***
897 (A, B) Transverse sections taken at multiple levels along the proximodistal axis from the limbs
898 shown in Fig. 5. The induced limbs exhibit dorsoventrally symmetric internal structures. Scale bar =
899 1 mm.
900
901 ***Figure S5. Gene expression patterns during normal limb regeneration.***
902 (A) Sections of amputation-induced blastemas at the early bud (EB), middle bud (MB), and late bud
903 (LB) stages. *Lmx1b*, *Wnt10b*, and *Fgf2* expression was visualized by *in situ* hybridization. (B)
904 Quantitative analysis of *Lmx1b*, *Wnt10b*, and *Fgf2* expression in MB-stage blastemas during normal
905 regeneration (n=13). Gene expression was quantified by RT-qPCR on manually microdissected
906 dorsal and ventral halves of each blastema. *p<0.05, **p<0.005 (two-tailed paired t-test). (C)
907 Quantitative analysis of *Wnt10b*, *Fgf2*, and *Shh* expression across stages (intact, EB, MB, LB, and
908 early digit [ED]; n = 5 for all stages). *Wnt10b* and *Fgf2* expression peaked at the MB stage, whereas
909 *Shh* expression peaked later, at the LB stage. One-way ANOVA detected a stage-dependent
910 difference ($p < 0.05$ for *Wnt10b* and *Fgf2*; $p < 0.001$ for *Shh*), followed by Dunnett's test. *p<0.05,
911 **p<0.005.
912
913 ***Figure S6. Gene expression patterns in a normal blastema assessed by reanalysis of axolotl***
914 ***single-cell RNA-seq data.***
915 Reanalysis of single-cell RNA-seq data from a middle bud (MB) stage blastema (Li et al., 2021).
916 (A–G) FeaturePlot visualizations of *Prrx1* (mesenchyme marker), *Krt17* (epithelium marker),

Lmx1b, *Wnt10b*, *Fgf2*, *Fgf8*, and *Shh*. *Lmx1b*, *Fgf2*, *Fgf8*, and *Shh* expression are detected in the mesenchymal cluster, whereas *Wnt10b* expression is detected in both mesenchymal and epithelial clusters. (H–M) "Co-expression" maps generated by classifying cells as expressing gene A only, gene B only, both genes, or neither gene, and overlaying these classes on the UMAP using DimPlot.

Table 1. The induction rate of bump/limb formation in ALM.

927 ***References***

928 Al Ghamdi, M. A., Al-Qattan, M. M., Hadadi, A., Alabdulrahman, A., Almuzzaini, B., Alatwi, N., &
929 AlBalwi, M. A. (2020). A classification system for split-hand/ foot malformation (SHFM): A
930 proposal based on 3 pedigrees with WNT10B mutations. European Journal of Medical Genetics,
931 63(3), 103738. https://doi.org/https://doi.org/10.1016/j.ejmg.2019.103738

932 Bennett, C. N., Longo, K. A., Wright, W. S., Suva, L. J., Lane, T. F., Hankenson, K. D., & MacDougald,
933 O. A. (2005). Regulation of osteoblastogenesis and bone mass by Wnt10b. Proceedings of the
934 National Academy of Sciences, 102(9), 3324–3329. https://doi.org/10.1073/pnas.0408742102

935 Berg, S., Kutra, D., Kroeger, T., Straehle, C. N., Kausler, B. X., Haubold, C., Schiegg, M., Ales, J.,
936 Beier, T., Rudy, M., Eren, K., Cervantes, J. I., Xu, B., Beuttenmueller, F., Wolny, A., Zhang, C.,
937 Koethe, U., Hamprecht, F. A., & Kreshuk, A. (2019). ilastik: interactive machine learning for
938 (bio)image analysis. Nature Methods, 16(12), 1226–1232. https://doi.org/10.1038/s41592-019-
939 0582-9

940 Bilal, M., Haack, T. B., Buchert, R., Peralta, S., Ahmad, I., Faisal, Abbasi, S., & Ahmad, W. (2023).
941 Sequence Variants in the WNT10B Underlying Non-Syndromic Split-Hand/Foot Malformation.
942 Molecular Syndromology, 14(6), 469–476. https://doi.org/10.1159/000531069

943 Bolger, A. M., Lohse, M., & Usadel, B. (2014). Trimmomatic: a flexible trimmer for Illumina sequence
944 data. Bioinformatics, 30(15), 2114–2120. https://doi.org/10.1093/bioinformatics/btu170

945 BRYANT, S. V. (1976). Regenerative failure of double half limbs in Notophthalmus viridescens.
946 Nature, 263(5579), 676–679. https://doi.org/10.1038/263676a0

947 Bryant, S. V, & Baca, B. A. (1978). Regenerative ability of double-half and half upper arms in the
948 newt, Notophthalmus viridescens. Journal of Experimental Zoology, 204(3), 307–323.
949 https://doi.org/https://doi.org/10.1002/jez.1402040302

950 Bryant, S. V, & Iten, L. E. (1976). Supernumerary limbs in amphibians: Experimental production in
951 Notophthalmus viridescens and a new interpretation of their formation. Developmental Biology,
952 50(1), 212–234. https://doi.org/https://doi.org/10.1016/0012-1606(76)90079-8

953 Burton, R., Holder, N., & Jesani, P. (1986). The regeneration of double dorsal and double ventral limbs
954 in the axolotl. Development, 94(1), 29–46. https://doi.org/10.1242/dev.94.1.29

955 Chen H, J. R. (2002). Interactions between dorsal-ventral patterning genes lmx1b, engrailed-1 and
956 wnt-7a in the vertebrate limb. Int J Dev Biol, 46(7), 937–941.

957 Chen, H., Lun, Y., Ovchinnikov, D., Kokubo, H., Oberg, K. C., Pepicelli, C. V, Can, L., Lee, B., &
958 Johnson, R. L. (1998). Limb and kidney defects in Lmx1b mutant mice suggest an involvement
959 of LMX1B in human nail patella syndrome. Nature Genetics, 19(1), 51–55.
960 https://doi.org/10.1038/ng0598-51

961 Cygan, J. A., Johnson, R. L., & McMahon, A. P. (1997). Novel regulatory interactions revealed by
962 studies of murine limb pattern in Wnt-7a and En-1 mutants. Development, 124(24), 5021–5032.

https://doi.org/10.1242/dev.124.24.5021

Endo, T., Bryant, S. V, & Gardiner, D. M. (2004). A stepwise model system for limb regeneration. Developmental Biology, 270(1), 135–145. https://doi.org/https://doi.org/10.1016/j.ydbio.2004.02.016

Endo, T., Gardiner, D. M., Makanae, A., & Satoh, A. (2015). The Accessory Limb Model: An Alternative Experimental System of Limb Regeneration. In A. Kumar & A. Simon (Eds.), Salamanders in Regeneration Research: Methods and Protocols (pp. 101–113). Springer New York. https://doi.org/10.1007/978-1-4939-2495-0_8

Gerber, T., Murawala, P., Knapp, D., Masselink, W., Schuez, M., Hermann, S., Gac-Santel, M., Nowoshilow, S., Kageyama, J., Khattak, S., Currie, J. D., Camp, J. G., Tanaka, E. M., & Treutlein, B. (2018). Single-cell analysis uncovers convergence of cell identities during axolotl limb regeneration. Science, 362(6413), eaaq0681. https://doi.org/10.1126/science.aaq0681

Giampaoli, S., Bucci, S., Ragghianti, M., Mancino, G., Zhang, F., & Ferretti, P. (2003). Expression of FGF2 in the limb blastema of two Salamandridae correlates with their regenerative capability. Proceedings of the Royal Society of London. Series B: Biological Sciences, 270(1530), 2197–2205. https://doi.org/10.1098/rspb.2003.2439

Glotzer, G. L., Tardivo, P., & Tanaka, E. M. (2022). Canonical Wnt signaling and the regulation of divergent mesenchymal Fgf8 expression in axolotl limb development and regeneration. ELife, 11, e79762. https://doi.org/10.7554/eLife.79762

Hao, Y., Hao, S., Andersen-Nissen, E., Mauck, W. M., Zheng, S., Butler, A., Lee, M. J., Wilk, A. J., Darby, C., Zager, M., Hoffman, P., Stoeckius, M., Papalexi, E., Mimitou, E. P., Jain, J., Srivastava, A., Stuart, T., Fleming, L. M., Yeung, B., … Satija, R. (2021). Integrated analysis of multimodal single-cell data. Cell, 184(13), 3573-3587.e29. https://doi.org/https://doi.org/10.1016/j.cell.2021.04.048

Hirata, A., Gardiner, D. M., & Satoh, A. (2010). Dermal fibroblasts contribute to multiple tissues in the accessory limb model. DGD, 52(4), 343–350. https://doi.org/https://doi.org/10.1111/j.1440-169X.2009.01165.x

Iten, L. E., & Bryant, S. V. (1975). The interaction between the blastema and stump in the establishment of the anterior-posterior and proximal-distal organization of the limb regenerate. Developmental Biology, 44(1), 119–147. https://doi.org/https://doi.org/10.1016/0012-1606(75)90381-4

Iwata, R., Makanae, A., & Satoh, A. (2020). Stability and plasticity of positional memory during limb regeneration in Ambystoma mexicanum. Developmental Dynamics, 249(3), 342–353. https://doi.org/https://doi.org/10.1002/dvdy.96

Kashimoto, R., Furukawa, S., Yamamoto, S., & Satoh, A. (2023). Bead Implantation and Delivery of Exogenous Growth Factors. In A. W. Seifert & J. D. Currie (Eds.), Salamanders: Methods and

Protocols (pp. 209–216). Springer US. https://doi.org/10.1007/978-1-0716-2659-7_14

Kawakami, Y., Rodriguez Esteban, C., Raya, M., Kawakami, H., Martí, M., Dubova, I., & Izpisúa Belmonte, J. C. (2006). Wnt/β-catenin signaling regulates vertebrate limb regeneration. Genes & Development, 20(23), 3232–3237. https://doi.org/10.1101/gad.1475106

Kim, D., Langmead, B., & Salzberg, S. L. (2015). HISAT: a fast spliced aligner with low memory requirements. Nature Methods, 12(4), 357–360. https://doi.org/10.1038/nmeth.3317

Kragl, M., Knapp, D., Nacu, E., Khattak, S., Maden, M., Epperlein, H. H., & Tanaka, E. M. (2009). Cells keep a memory of their tissue origin during axolotl limb regeneration. Nature, 460(7251), 60–65. https://doi.org/10.1038/nature08152

Laufer, E., Nelson, C. E., Johnson, R. L., Morgan, B. A., & Tabin, C. (1994). Sonic hedgehog and Fgf-4 act through a signaling cascade and feedback loop to integrate growth and patterning of the developing limb bud. Cell, 79(6), 993–1003. https://doi.org/https://doi.org/10.1016/0092-8674(94)90030-2

Lévesque, M., Gatien, S., Finnson, K., Desmeules, S., Villiard, É., Pilote, M., Philip, A., & Roy, S. (2007). Transforming Growth Factor: β Signaling Is Essential for Limb Regeneration in Axolotls. PLOS ONE, 2(11), e1227-. https://doi.org/10.1371/journal.pone.0001227

Li, H., Wei, X., Zhou, L., Zhang, W., Wang, C., Guo, Y., Li, D., Chen, J., Liu, T., Zhang, Y., Ma, S., Wang, C., Tan, F., Xu, J., Liu, Y., Yuan, Y., Chen, L., Wang, Q., Qu, J., … Xu, X. (2021). Dynamic cell transition and immune response landscapes of axolotl limb regeneration revealed by single-cell analysis. Protein & Cell, 12(1), 57–66. https://doi.org/10.1007/s13238-020-00763-1

Li, Q., Kannan, A., Das, A., DeMayo, F. J., Hornsby, P. J., Young, S. L., Taylor, R. N., Bagchi, M. K., & Bagchi, I. C. (2013). WNT4 Acts Downstream of BMP2 and Functions via β-Catenin Signaling Pathway to Regulate Human Endometrial Stromal Cell Differentiation. Endocrinology, 154(1), 446–457. https://doi.org/10.1210/en.2012-1585

Li, S., Anderson, R., Reginelli, A. D., & Muneoka, K. (1996). FGF-2 influences cell movements and gene expression during limb development. Journal of Experimental Zoology, 274(4), 234–247. https://doi.org/https://doi.org/10.1002/(SICI)1097-010X(19960301)274:4<234::AID-JEZ4>3.0.CO;2-Q

Li, X., Li, Z., Wang, J., Li, Z., Cui, H., Dai, G., Chen, S., Zhang, M., Zheng, Z., Zhan, Z., & Liu, H. (2019). Wnt4 signaling mediates protective effects of melatonin on new bone formation in an inflammatory environment. The FASEB Journal, 33(9), 10126–10139. https://doi.org/https://doi.org/10.1096/fj.201900093RR

Liao, Y., Smyth, G. K., & Shi, W. (2014). featureCounts: an efficient general purpose program for assigning sequence reads to genomic features. Bioinformatics, 30(7), 923–930. https://doi.org/10.1093/bioinformatics/btt656

Lin, Y.-C., Haas, A., Bufe, A., Parbin, S., Hennecke, M., Voloshanenko, O., Gross, J., Boutros, M.,

Acebron, S. P., & Bastians, H. (2021). Wnt10b-GSK3β–dependent Wnt/STOP signaling prevents aneuploidy in human somatic cells. Life Science Alliance, 4(1), e202000855. https://doi.org/10.26508/lsa.202000855

Logan, C., Hornbruch, A., Campbell, I., & Lumsden, A. (1997). The role of Engrailed in establishing the dorsoventral axis of the chick limb. Development, 124(12), 2317–2324. https://doi.org/10.1242/dev.124.12.2317

Loomis, C. A., Harris, E., Michaud, J., Wurst, W., Hanks, M., & Joyner, A. L. (1996). The mouse Engrailed-1 gene and ventral limb patterning. Nature, 382(6589), 360–363. https://doi.org/10.1038/382360a0

Love, M. I., Huber, W., & Anders, S. (2014). Moderated estimation of fold change and dispersion for RNA-seq data with DESeq2. Genome Biology, 15(12), 550. https://doi.org/10.1186/s13059-014-0550-8

Lovely, A. M., Duerr, T. J., Qiu, Q., Galvan, S., Voss, S. R., & Monaghan, J. R. (2022). Wnt Signaling Coordinates the Expression of Limb Patterning Genes During Axolotl Forelimb Development and Regeneration. Frontiers in Cell and Developmental Biology, 10. https://www.frontiersin.org/journals/cell-and-developmental-biology/articles/10.3389/fcell.2022.814250

Ludolph, D. C., Cameron, J. A., & Stocum, D. L. (1990). The effect of retinoic acid on positional memory in the dorsoventral axis of regenerating axolotl limbs. Developmental Biology, 140(1), 41–52. https://doi.org/https://doi.org/10.1016/0012-1606(90)90051-J

Maden, M. (1980). Structure of supernumerary limbs. Nature, 286(5775), 803–805. https://doi.org/10.1038/286803a0

Makanae, A., Mitogawa, K., & Satoh, A. (2014a). Co-operative Bmp- and Fgf-signaling inputs convert skin wound healing to limb formation in urodele amphibians. Developmental Biology, 396(1), 57–66. https://doi.org/https://doi.org/10.1016/j.ydbio.2014.09.021

Makanae, A., Mitogawa, K., & Satoh, A. (2014b). Implication of two different regeneration systems in limb regeneration. Regeneration, 1(3), 1–9. https://doi.org/https://doi.org/10.1002/reg2.16

McCusker, C., Lehrberg, J., & Gardiner, D. (2014). Position-specific induction of ectopic limbs in non-regenerating blastemas on axolotl forelimbs. Regeneration, 1(1), 27–34. https://doi.org/https://doi.org/10.1002/reg2.10

Mescher, A. L. (1976). Effects on adult newt limb regeneration of partial and complete skin flaps over the amputation surface. Journal of Experimental Zoology, 195(1), 117–127. https://doi.org/https://doi.org/10.1002/jez.1401950111

Muneoka, K., Fox, W. F., & Bryant, S. V. (1986). Cellular contribution from dermis and cartilage to the regenerating limb blastema in axolotls. Developmental Biology, 116(1), 256–260. https://doi.org/https://doi.org/10.1016/0012-1606(86)90062-X

Nacu, E., Gromberg, E., Oliveira, C. R., Drechsel, D., & Tanaka, E. M. (2016). FGF8 and SHH substitute for anterior–posterior tissue interactions to induce limb regeneration. Nature, 533(7603), 407–410. https://doi.org/10.1038/nature17972

Niswander, L., Jeffrey, S., Martin, G. R., & Tickle, C. (1994). A positive feedback loop coordinates growth and patterning in the vertebrate limb. Nature, 371(6498), 609–612. https://doi.org/10.1038/371609a0

Otsuki, L., & Tanaka, E. (2021). Positional Memory in Vertebrate Regeneration: A Century's Insights from the Salamander Limb. Cold Spring Harbor Perspectives in Biology, 14, a040899. https://doi.org/10.1101/cshperspect.a040899

Parr, B. A., & McMahon, A. P. (1995). Dorsalizing signal Wnt-7a required for normal polarity of D–V and A–P axes of mouse limb. Nature, 374(6520), 350–353. https://doi.org/10.1038/374350a0

Patro, R., Duggal, G., Love, M. I., Irizarry, R. A., & Kingsford, C. (2017). Salmon provides fast and bias-aware quantification of transcript expression. Nature Methods, 14(4), 417–419. https://doi.org/10.1038/nmeth.4197

Poulin, M. L., Patrie, K. M., Botelho, M. J., Tassava, R. A., & Chiu, I.-M. (1993). Heterogeneity in the expression of fibroblast growth factor receptors during limb regeneration in newts (Notophthalmus viridescens). Development, 119(2), 353–361. https://doi.org/10.1242/dev.119.2.353

Riddle, R. D., Ensini, M., Nelson, C., Tsuchida, T., Jessell, T. M., & Tabin, C. (1995). Induction of the LIM homeobox gene Lmx1 by WNT6a establishes dorsoventral pattern in the vertebrate limb. Cell, 83(4), 631–640. https://doi.org/https://doi.org/10.1016/0092-8674(95)90103-5

Riddle, R. D., Johnson, R. L., Laufer, E., & Tabin, C. (1993). Sonic hedgehog mediates the polarizing activity of the ZPA. Cell, 75(7), 1401–1416. https://doi.org/https://doi.org/10.1016/0092-8674(93)90626-2

Sader, F., & Roy, S. (2022). Tgf-β superfamily and limb regeneration: Tgf-β to start and Bmp to end. Developmental Dynamics, 251(6), 973–987. https://doi.org/https://doi.org/10.1002/dvdy.379

Satoh, A., Cummings, G. M. C., Bryant, S. V, & Gardiner, D. M. (2010). Regulation of proximal-distal intercalation during limb regeneration in the axolotl (Ambystoma mexicanum). Development, Growth & Differentiation, 52(9), 785–798. https://doi.org/https://doi.org/10.1111/j.1440-169X.2010.01214.x

Satoh, A., Gardiner, D. M., Bryant, S. V, & Endo, T. (2007). Nerve-induced ectopic limb blastemas in the axolotl are equivalent to amputation-induced blastemas. Developmental Biology, 312(1), 231–244. https://doi.org/https://doi.org/10.1016/j.ydbio.2007.09.021

Satoh, A., Makanae, A., Nishimoto, Y., & Mitogawa, K. (2016). FGF and BMP derived from dorsal root ganglia regulate blastema induction in limb regeneration in Ambystoma mexicanum. Developmental Biology, 417(1), 114–125.

https://doi.org/https://doi.org/10.1016/j.ydbio.2016.07.005

Schloissnig, S., Kawaguchi, A., Nowoshilow, S., Falcon, F., Otsuki, L., Tardivo, P., Timoshevskaya, N., Keinath, M. C., Smith, J. J., Voss, S. R., & Tanaka, E. M. (2021). The giant axolotl genome uncovers the evolution, scaling, and transcriptional control of complex gene loci. Proceedings of the National Academy of Sciences, 118(15), e2017176118. https://doi.org/10.1073/pnas.2017176118

SHIMOKAWA, T., YASUTAKA, S., KOMINAMI, R., & SHINOHARA, H. (2013). Lmx-1b and Wnt-7a expression in axolotl limb during development and regeneration. Okajimas Folia Anatomica Japonica, 89(4), 119–124. https://doi.org/10.2535/ofaj.89.119

Srivastava, A., Malik, L., Smith, T., Sudbery, I., & Patro, R. (2019). Alevin efficiently estimates accurate gene abundances from dscRNA-seq data. Genome Biology, 20(1), 65. https://doi.org/10.1186/s13059-019-1670-y

Stocum, D. L. (1982). Determination of axial polarity in the urodele limb regeneration blastema. Development, 71(1), 193–214. https://doi.org/10.1242/dev.71.1.193

Thomas, P. D., Kejariwal, A., Campbell, M. J., Mi, H., Diemer, K., Guo, N., Ladunga, I., Ulitsky-Lazareva, B., Muruganujan, A., Rabkin, S., Vandergriff, J. A., & Doremieux, O. (2003). PANTHER: a browsable database of gene products organized by biological function, using curated protein family and subfamily classification. Nucleic Acids Research, 31(1), 334–341. https://doi.org/10.1093/nar/gkg115

Thornton, C. S. (1962). Influence of head skin on limb regeneration in urodele amphibians. Journal of Experimental Zoology, 150(1), 5–15. https://doi.org/https://doi.org/10.1002/jez.1401500103

Todd, T. (1823). On the process of reproduction of the members of the aquatic salamander. Quart J Sci Lit Arts Lib, 16, 84–86.

Tsai, S. (2020). Inhibition of Wound Epidermis Formation via Full Skin Flap Surgery During Axolotl Limb Regeneration. JoVE, 160, e61522. https://doi.org/doi:10.3791/61522

Ugur, S. A., & Tolun, A. (2008). Homozygous WNT10b mutation and complex inheritance in Split-Hand/Foot Malformation. Human Molecular Genetics, 17(17), 2644–2653. https://doi.org/10.1093/hmg/ddn164

Vieira, W. A., Wells, K. M., Raymond, M. J., De Souza, L., Garcia, E., & McCusker, C. D. (2019). FGF, BMP, and RA signaling are sufficient for the induction of complete limb regeneration from non-regenerating wounds on Ambystoma mexicanum limbs. Developmental Biology, 451(2), 146–157. https://doi.org/https://doi.org/10.1016/j.ydbio.2019.04.008

Vogel, A., Rodriguez, C., Warnken, W., & Belmonte, J. C. I. (1995). Dorsal cell fate specified by chick Lmxl during vertebrate limb development. Nature, 378(6558), 716–720. https://doi.org/10.1038/378716a0

Voss, J. H., Koszegi, Z., Yan, Y., Shorter, E., Grätz, L., Lanner, J. T., Calebiro, D., & Schulte, G. (2025).

WNT-induced association of Frizzled and LRP6 is not sufficient for the initiation of WNT/β-catenin signaling. Nature Communications, 16(1), 4848. https://doi.org/10.1038/s41467-025-60096-7

Witte, F., Dokas, J., Neuendorf, F., Mundlos, S., & Stricker, S. (2009). Comprehensive expression analysis of all Wnt genes and their major secreted antagonists during mouse limb development and cartilage differentiation. Gene Expression Patterns, 9(4), 215–223. https://doi.org/https://doi.org/10.1016/j.gep.2008.12.009

Yamamoto, S., Kashimoto, R., Furukawa, S., Ohashi, A., & Satoh, A. (2022). Lmx1b activation in axolotl limb regeneration. Developmental Dynamics, 251(9), 1509–1523. https://doi.org/https://doi.org/10.1002/dvdy.476

Yang, Y., & Niswander, L. (1995). Interaction between the signaling molecules WNT7a and SHH during vertebrate limb development: Dorsal signals regulate anteroposterior patterning. Cell, 80(6), 939–947. https://doi.org/https://doi.org/10.1016/0092-8674(95)90297-X

Yonei-Tamura, S., Endo, T., Yajima, H., Ohuchi, H., Ide, H., & Tamura, K. (1999). FGF7 and FGF10 Directly Induce the Apical Ectodermal Ridge in Chick Embryos. Developmental Biology, 211(1), 133–143. https://doi.org/https://doi.org/10.1006/dbio.1999.9290

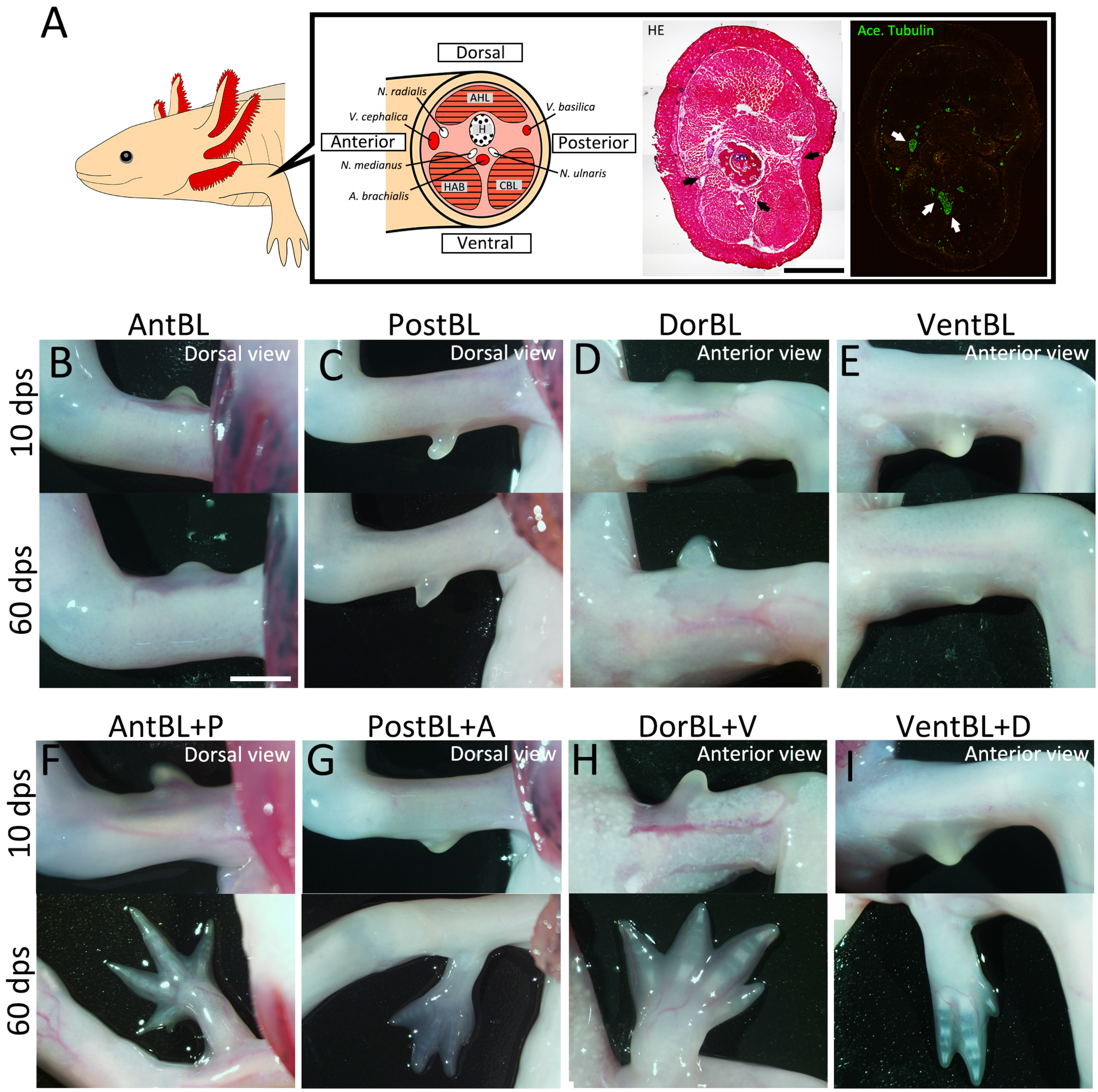

Yamamoto et al., 2025, Figure 1

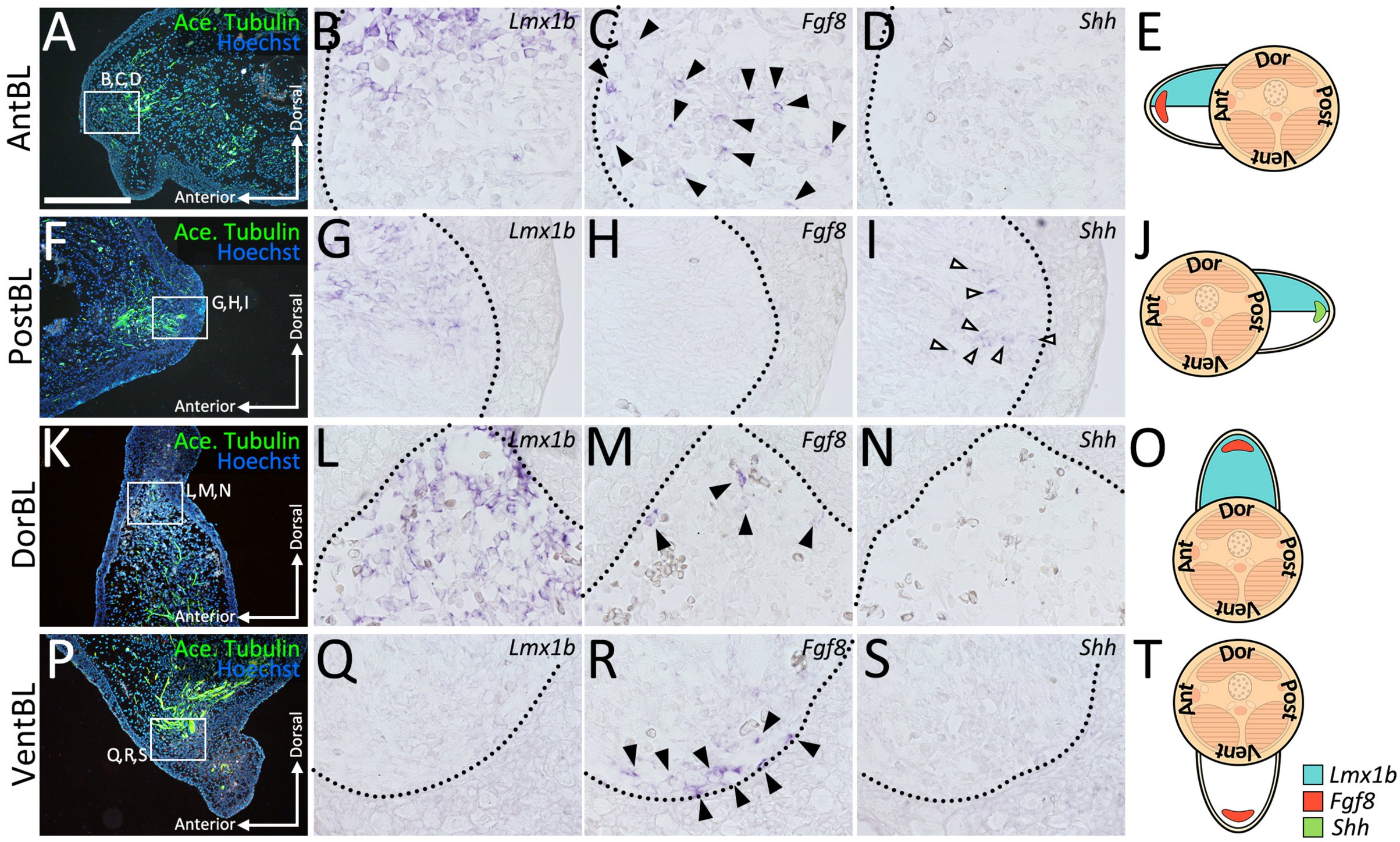

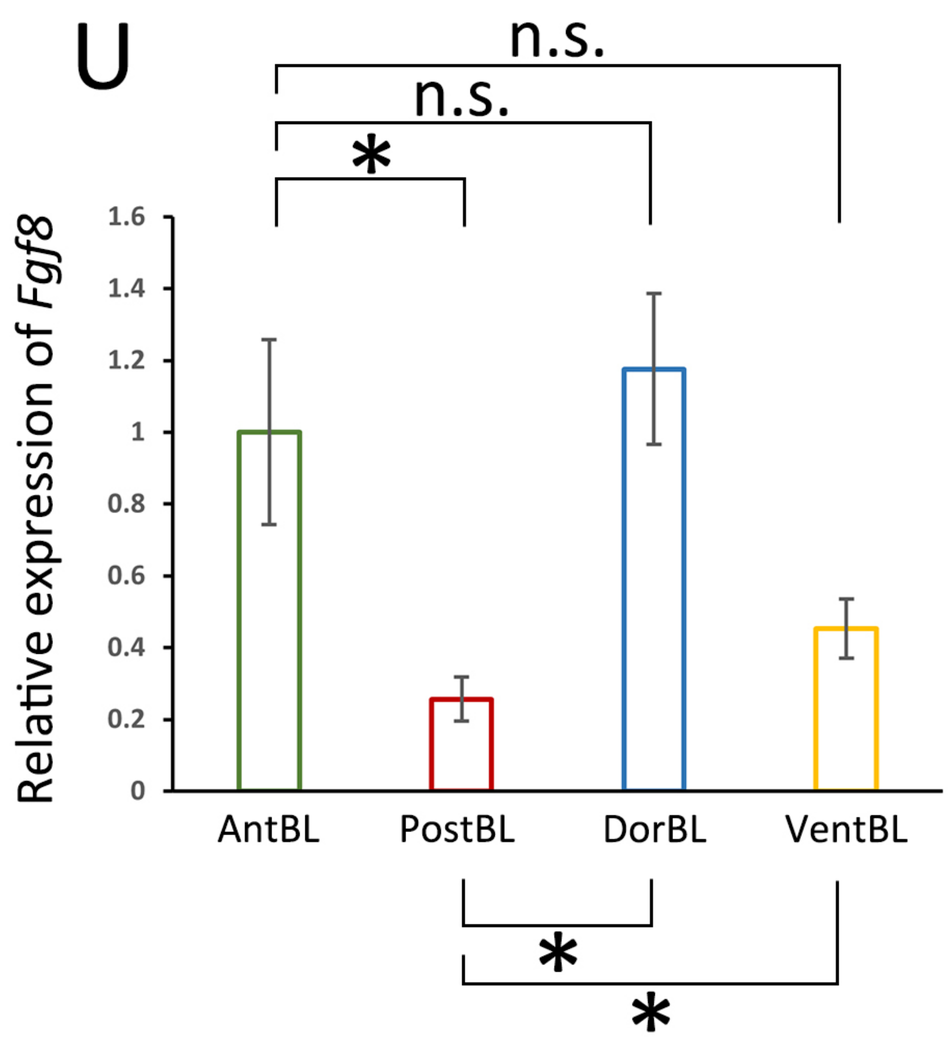

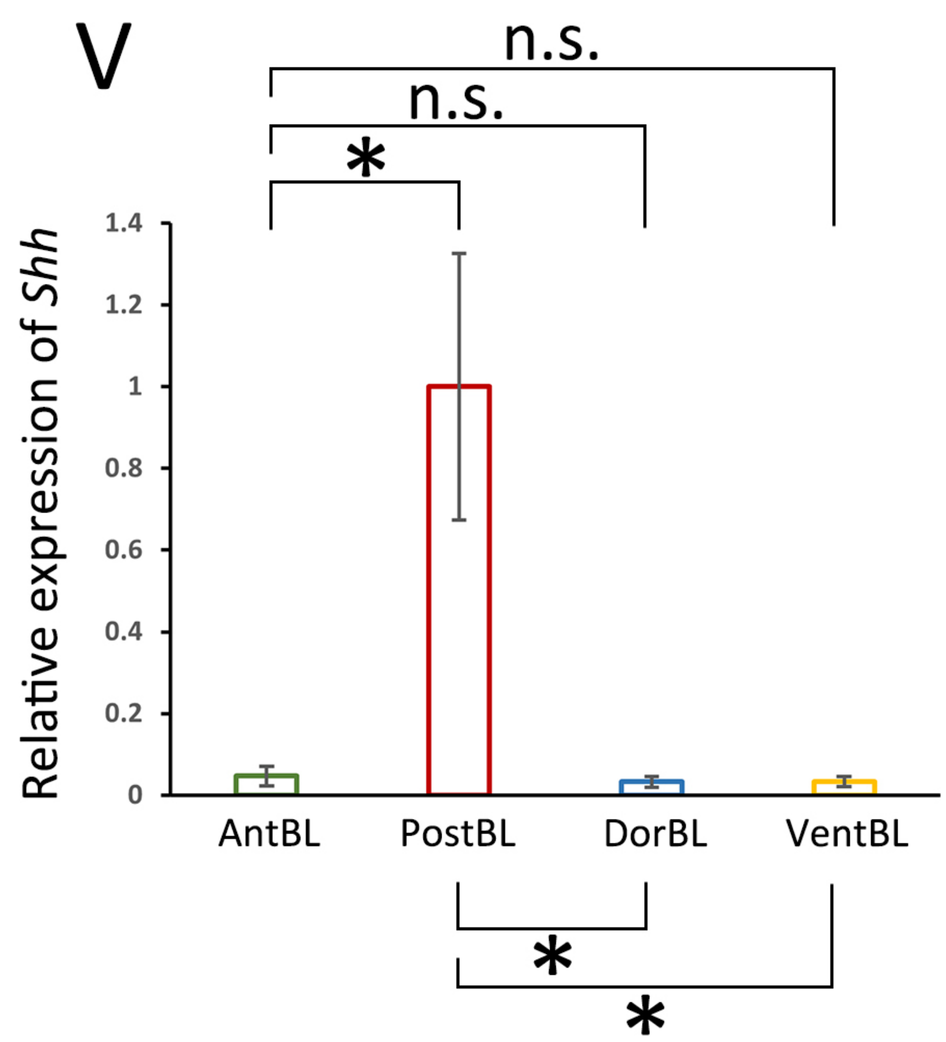

Yamamoto et al., 2025, Figure 2

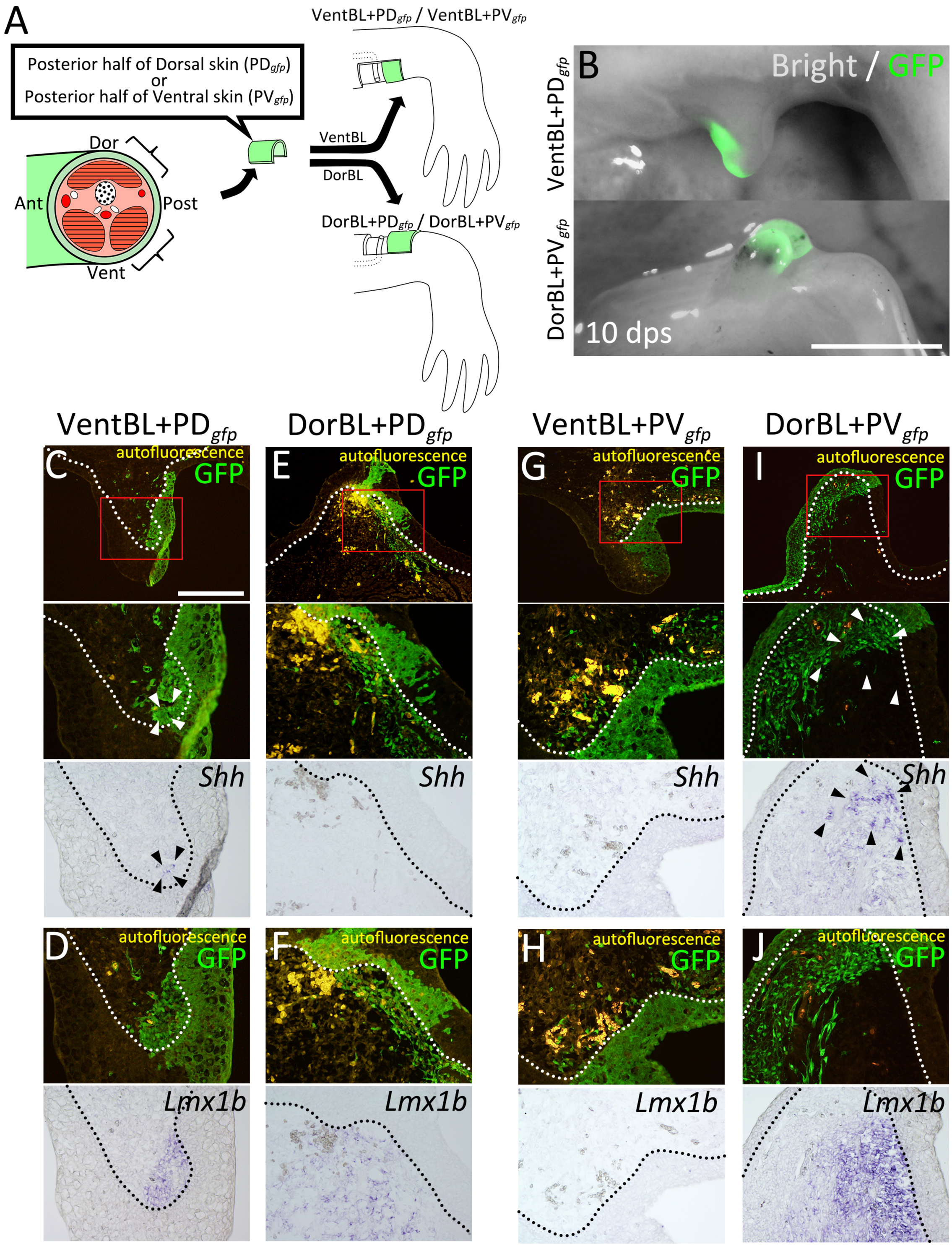

Yamamoto et al., 2025, Figure 3

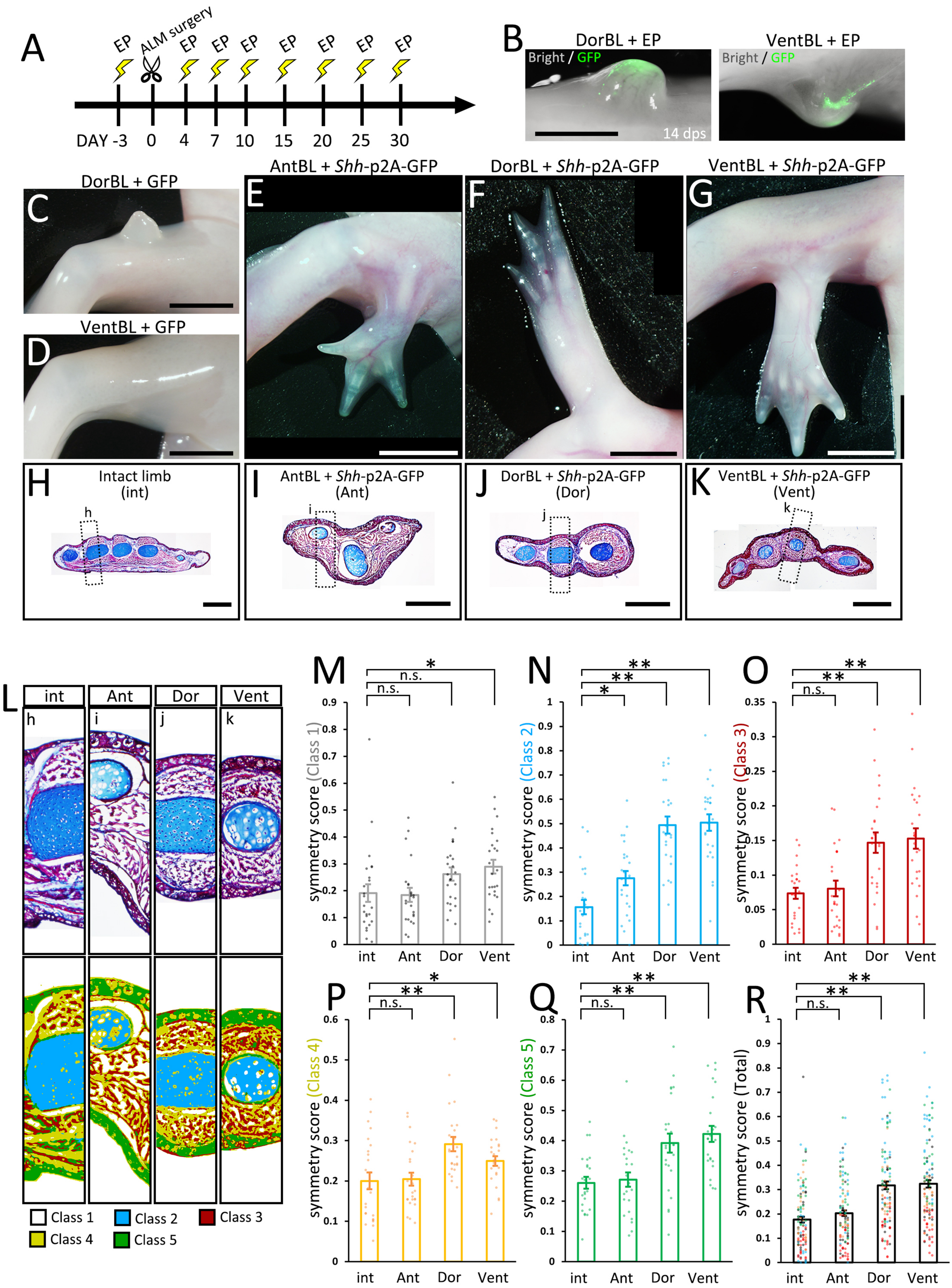

Yamamoto et al., 2025, Figure 4

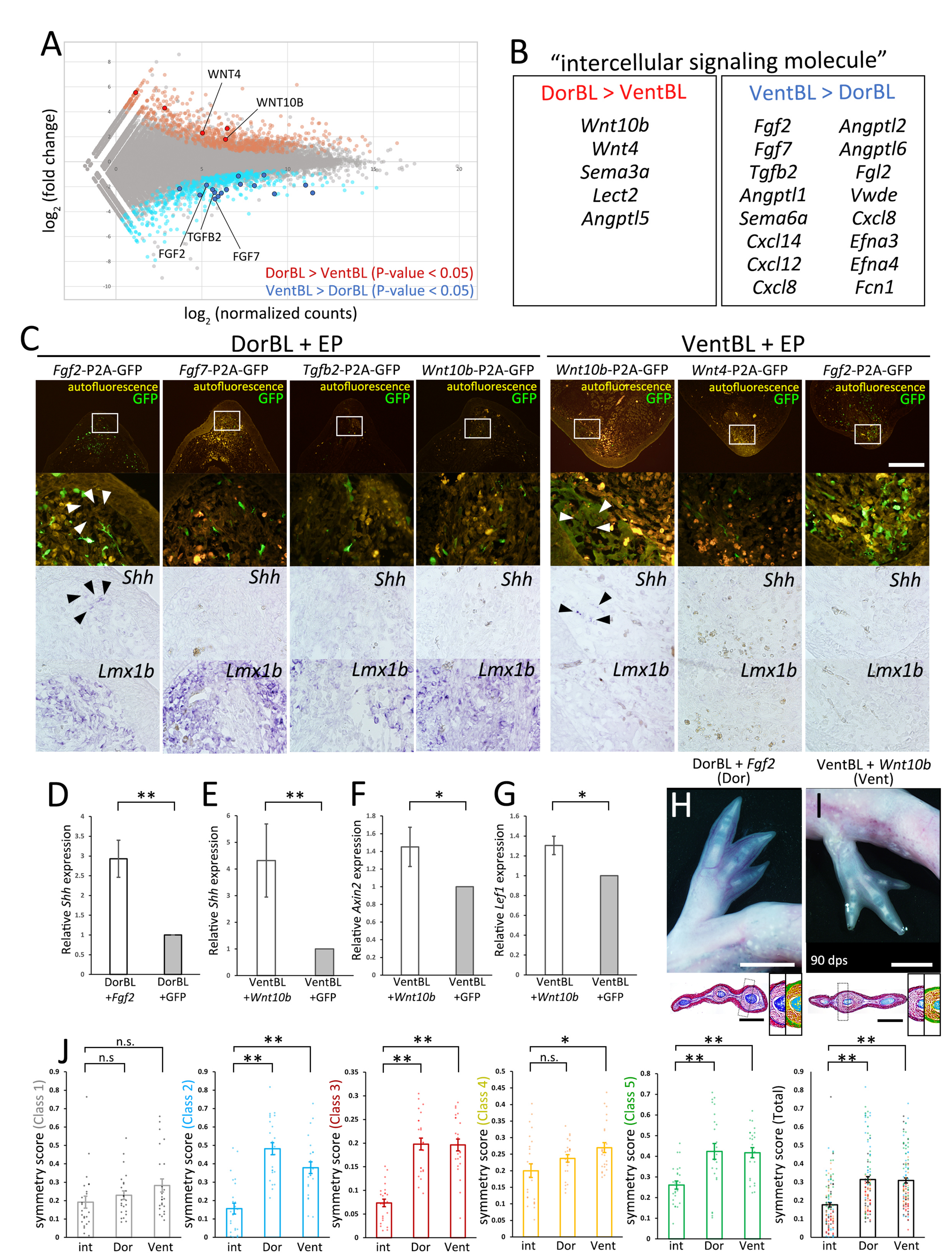

Yamamoto et al., 2025, Figure 5

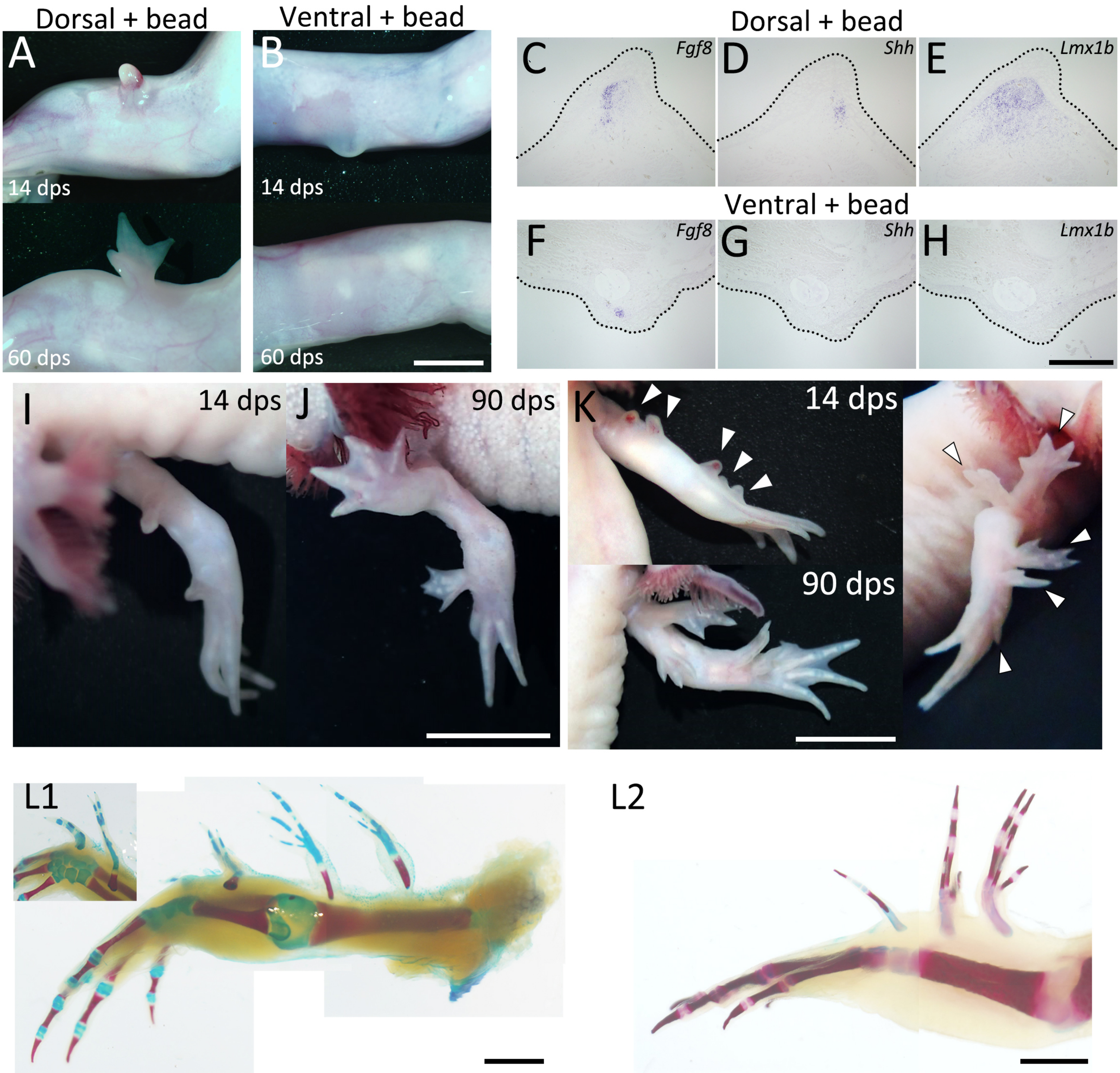

Yamamoto et al., 2025, Figure 6

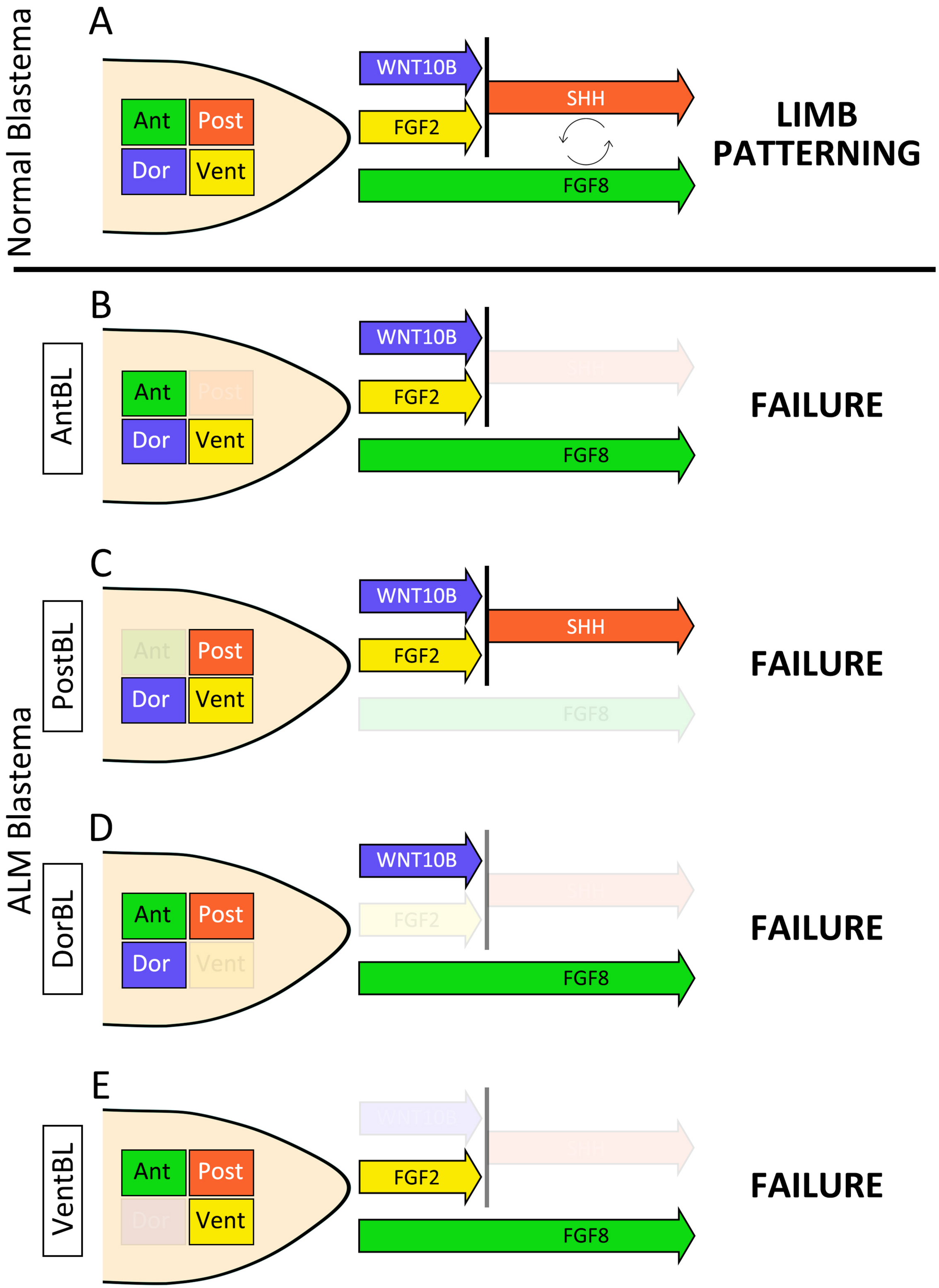

Yamamoto et al., 2025, Figure 7

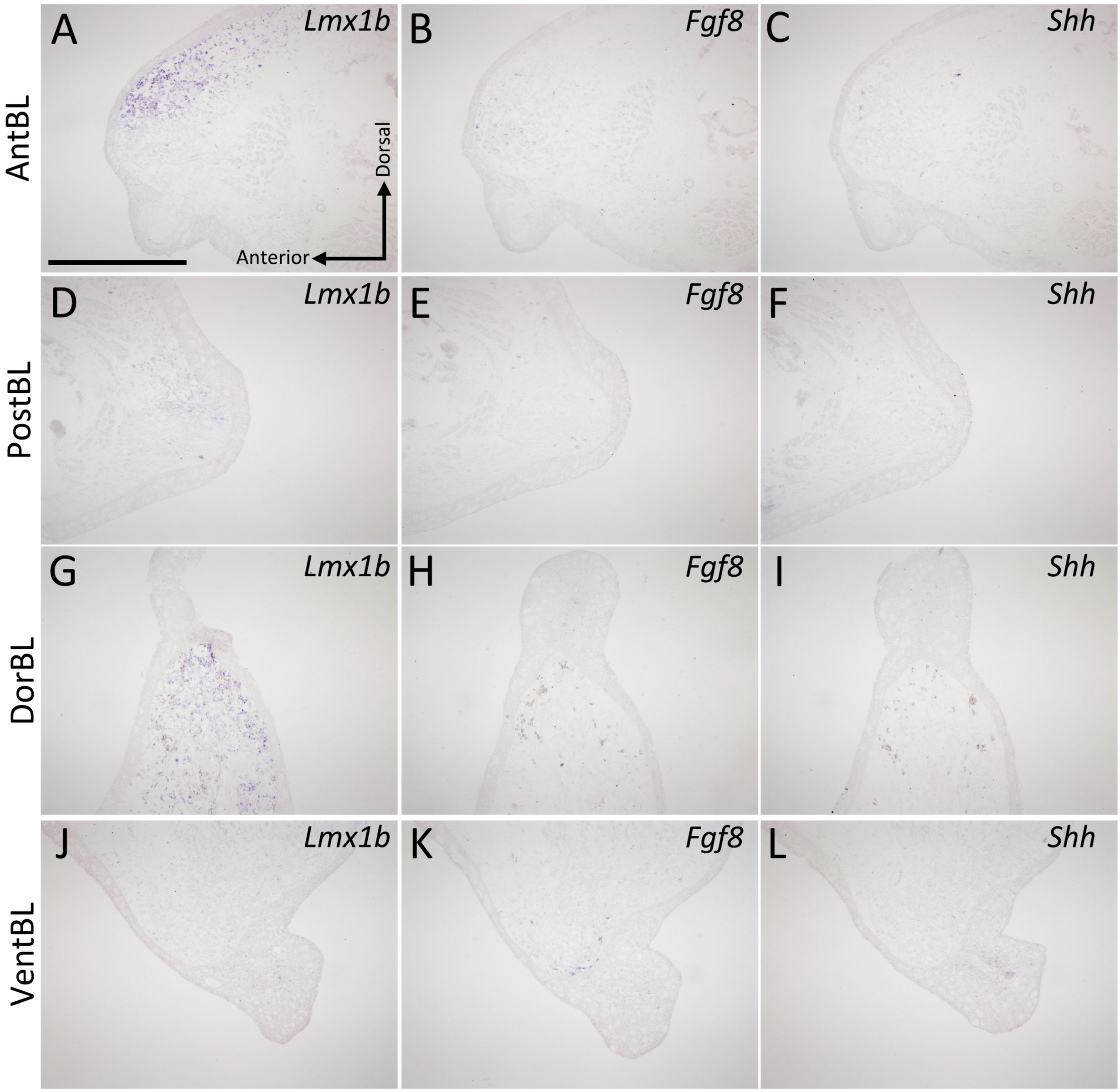

Yamamoto et al., 2025, Supplemental Figure 1

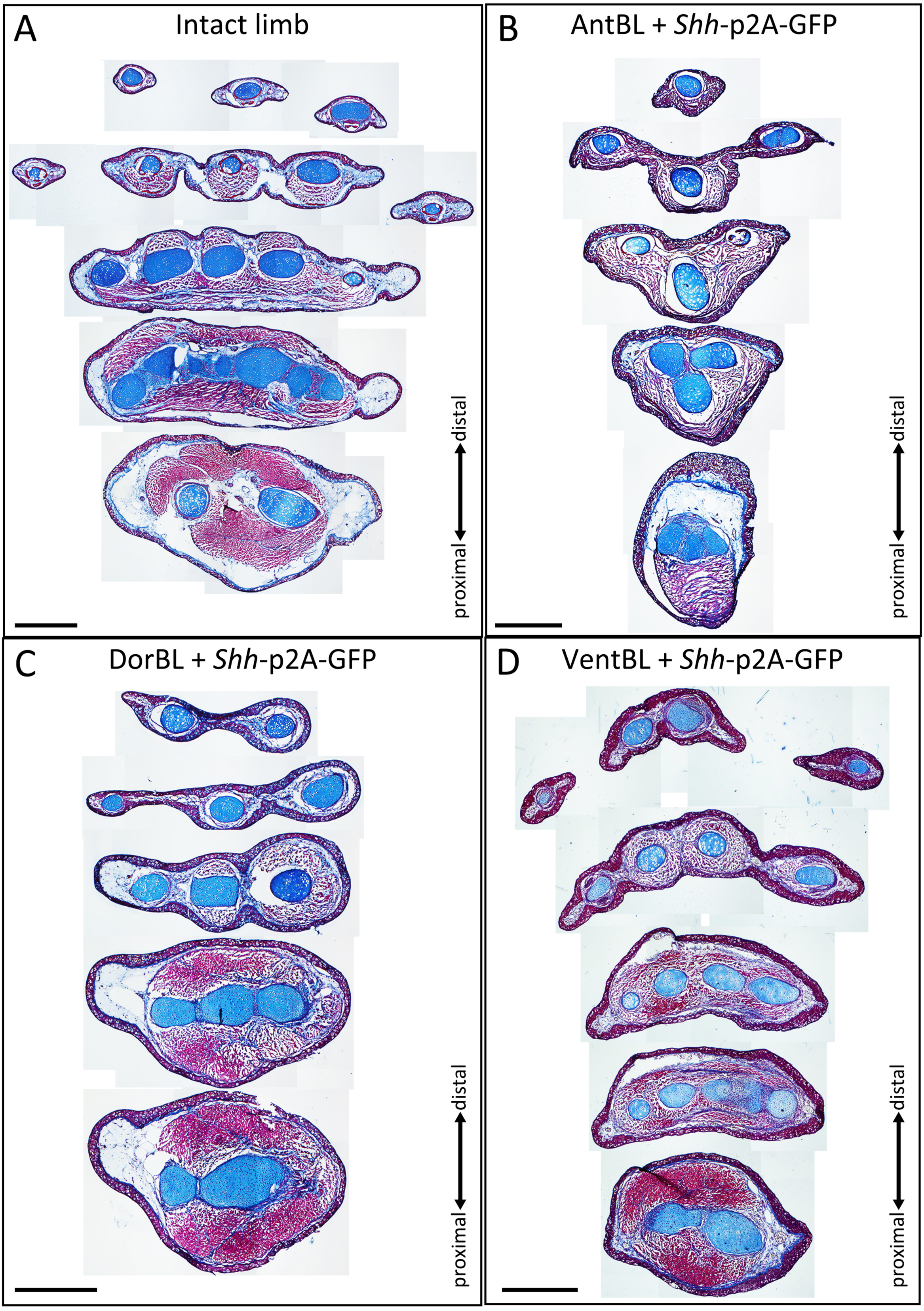

Yamamoto et al., 2025, Supplemental Figure 2

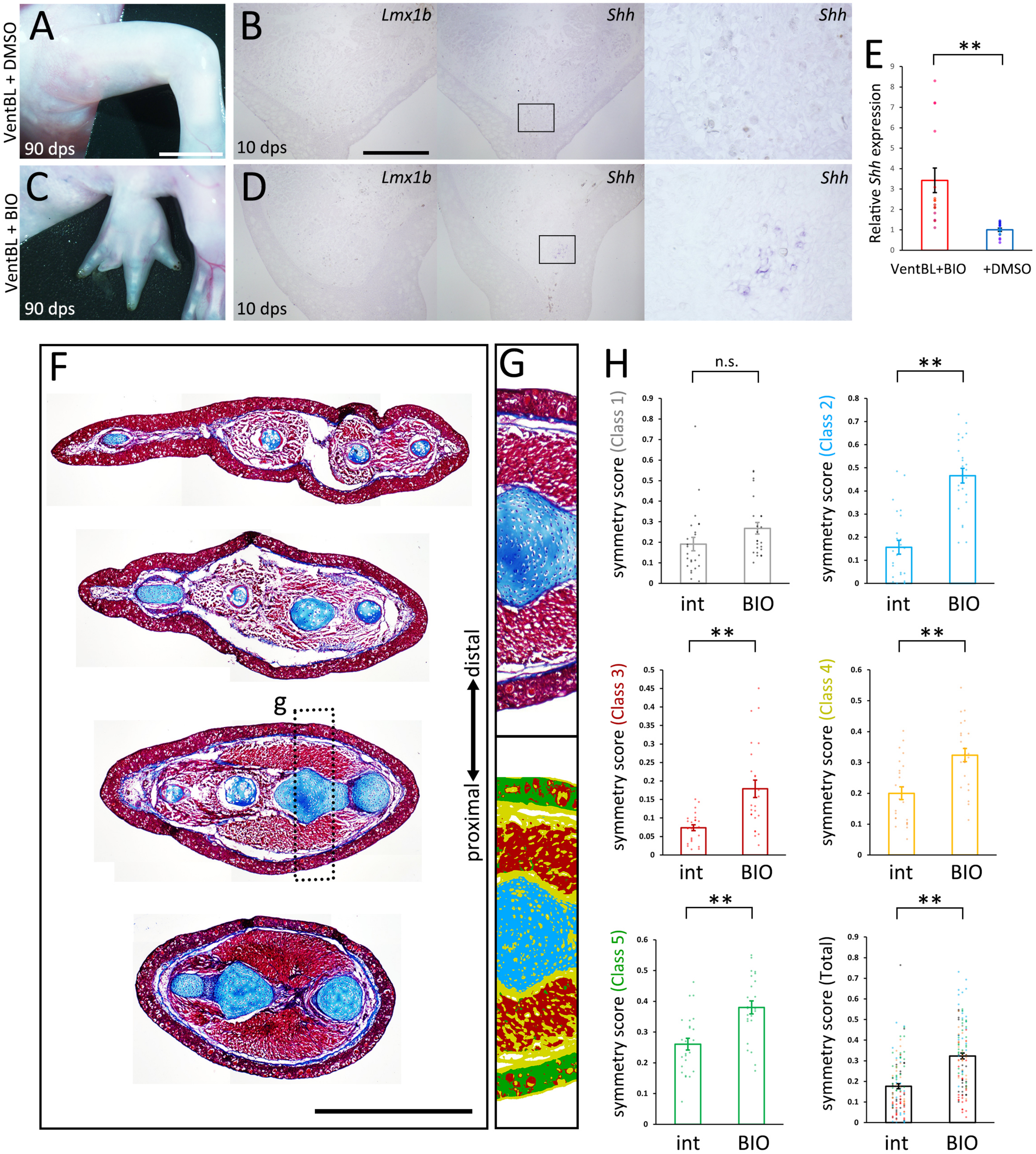

Yamamoto et al., 2025, Supplemental Figure 3

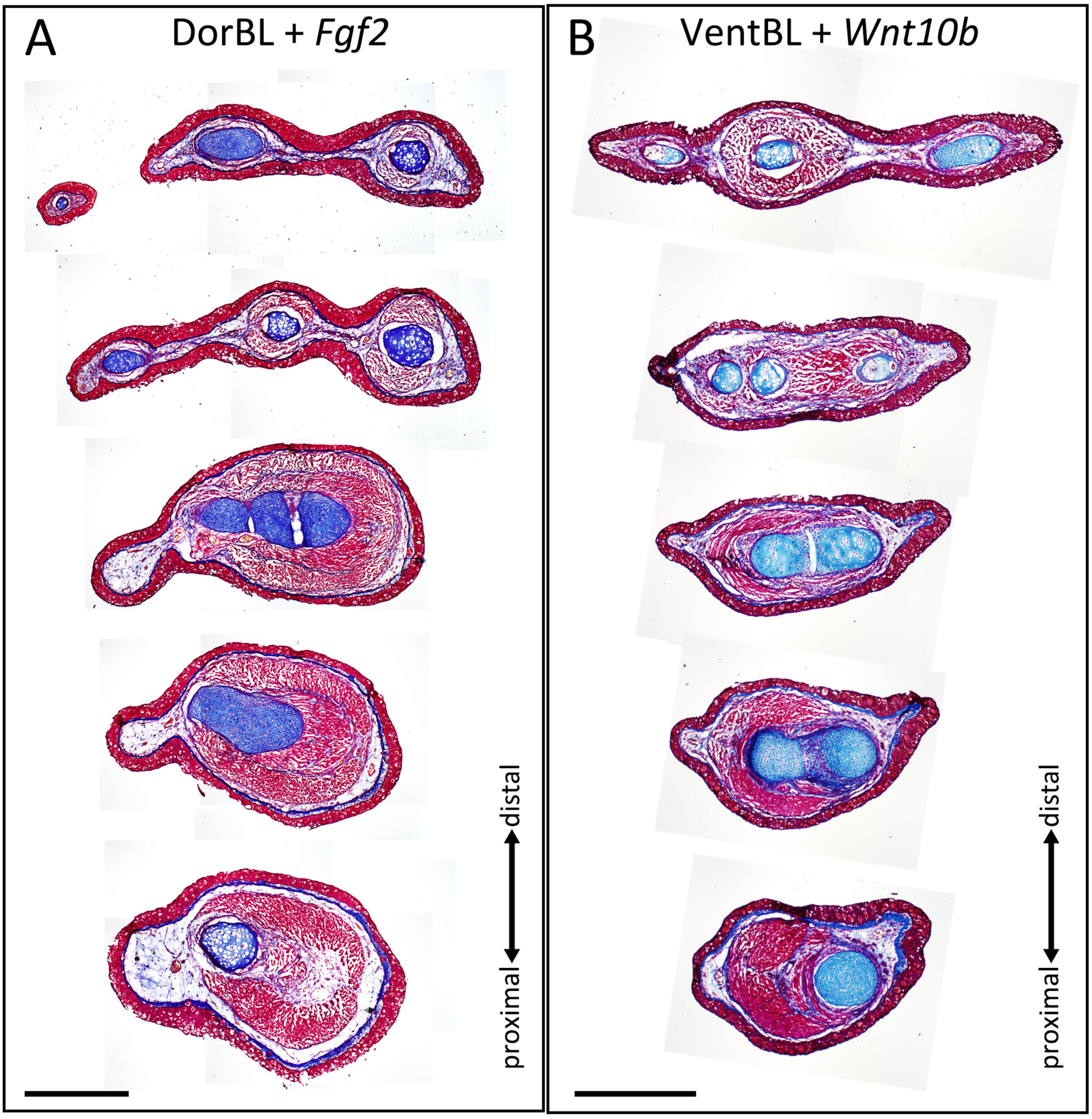

Yamamoto et al., 2025, Supplemental Figure 4

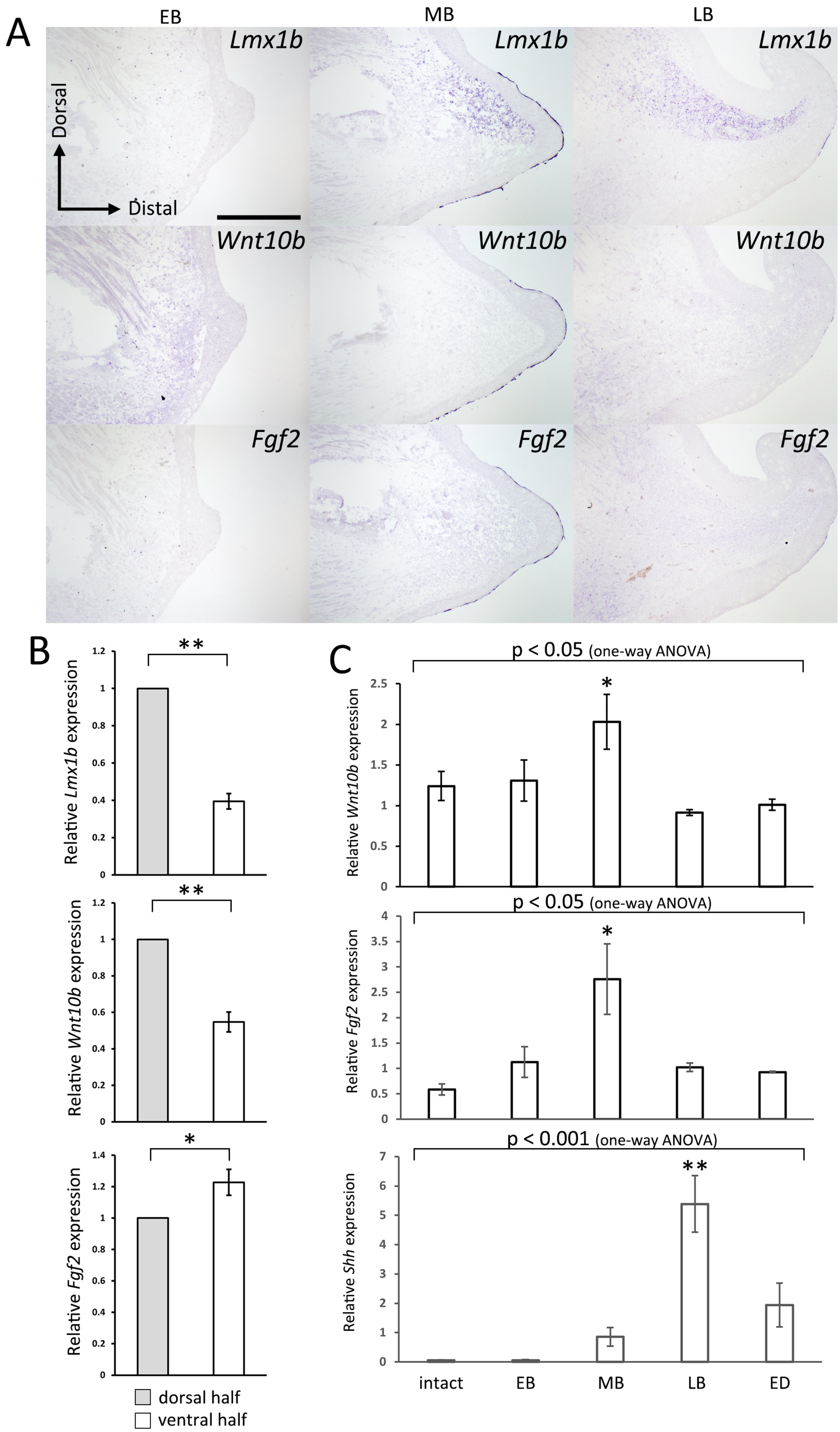

Yamamoto et al., 2025, Supplemental Figure 5

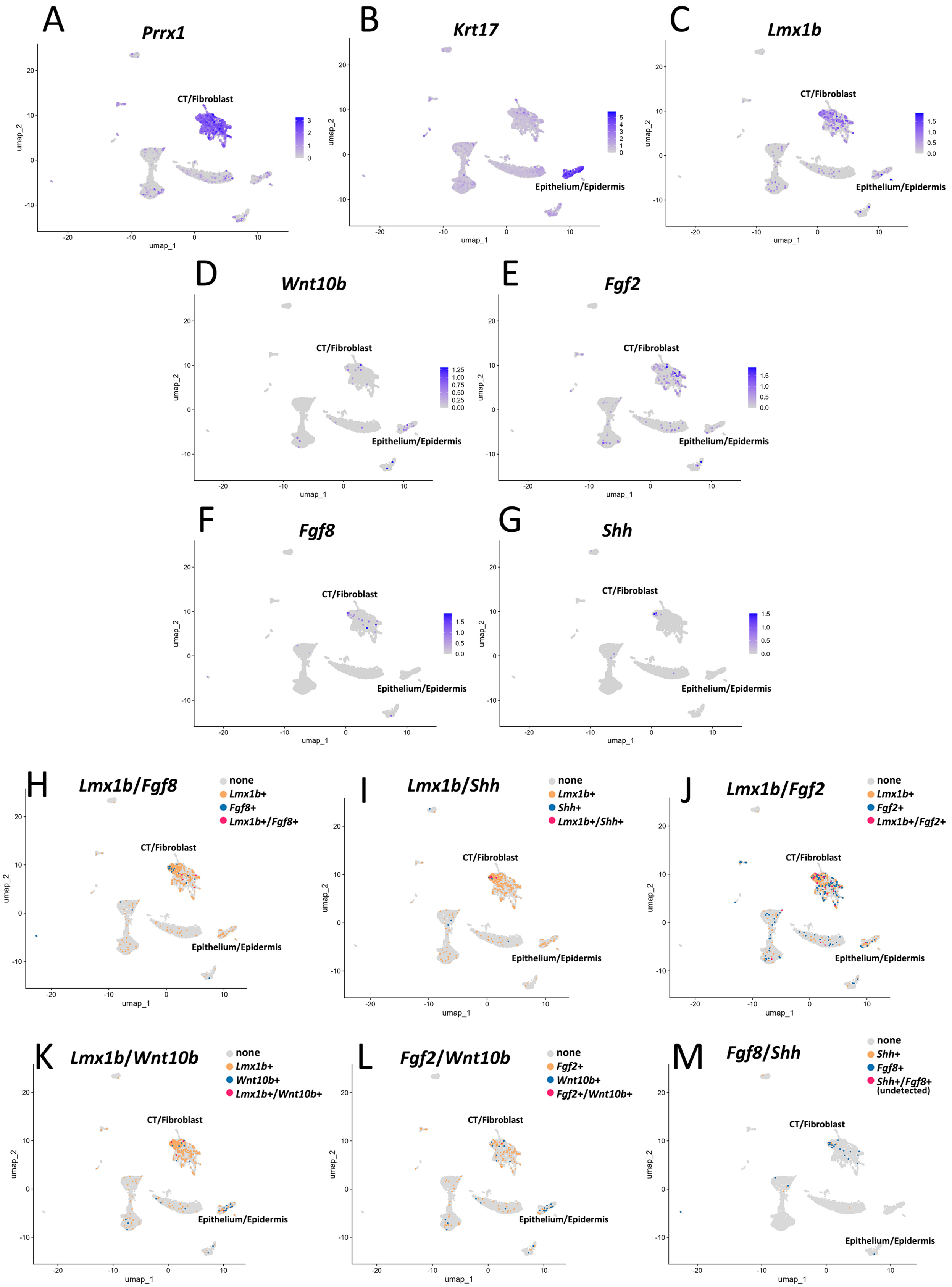

Yamamoto et al., 2025, Supplemental Figure 6

	N	**Regress**		**Bump**		**Limb**	
AntBL	8	3	(37.5 %)	5	(62.5 %)	0	(0.0 %)
AntBL+P	9	0	(0.0 %)	1	(11.1 %)	8	(88.9 %)
PostBL	8	6	(75.0 %)	2	(25.0 %)	0	(0.0 %)
PostBL+A	7	2	(28.6 %)	1	(14.3 %)	4	(57.1 %)
DorBL	12	8	(66.7 %)	3	(25.0 %)	1	(8.3 %)
DorBL+V	14	5	(35.7 %)	2	(14.3 %)	7	(50.0 %)
VentBL	22	15	(68.2 %)	7	(31.8 %)	0	(0.0 %)
VentBL+D	11	2	(18.2 %)	2	(18.2 %)	7	(63.6 %)